Chair of Mining Engineering and Mineral Economics

Master's Thesis

A DEM model for elastic sleepers to study dynamic railway track behaviour

Paul Pircher, BSc.

November 2021

MONTANUNIVERSITÄT LEOBEN
www.unileoben.ac.at

AFFIDAVIT

I declare on oath that I wrote this thesis independently, did not use other than the specified sources and aids, and did not otherwise use any unauthorized aids.

I declare that I have read, understood, and complied with the guidelines of the senate of the Montanuniversität Leoben for "Good Scientific Practice".

Furthermore, I declare that the electronic and printed version of the submitted thesis are identical, both, formally and with regard to content.

Date 01.11.2021

Signature Author
Paul Pircher

Title:	A DEM model for elastic sleepers to study dynamic railway track behaviour
Author:	Paul Pircher
Year / Place:	2021 / Graz, Austria
DOI:	https://doi.org/10.34901/mul.pub.2021.5

A master's thesis conducted in cooperation with

Virtual Vehicle Research GmbH

Inffeldgasse 21a
8010 Graz, Austria

Submitted by
Paul Pircher, BSc.

Supervisors:

Nikolaus August Sifferlinger (*Montanuniversität Leoben*)
Eric Fimbinger (*Montanuniversität Leoben*)
Klaus Six (*Virtual Vehicle*)
Nishant Kumar (*Virtual Vehicle*)

Copyright declaration

Acknowledgements

At this point, I personally want to thank everyone who supported me in writing this thesis.

Foremost, I would like to express my sincere gratitude to my mentor, supervisor and friend Nishant Kumar. Thanks for the best possible support I could imagine, for the endless time you took to advise me and for our numerous discussions that led to this work. Thank you also for your guidance and your support besides the technical, work-related aspects. Your extraordinary contribution to this thesis is profoundly appreciated.

Furthermore, I want to thank my supervisor, Klaus Six. Thank you for initially enabling me at Virtual Vehicle. Thank you for your guidance and for keeping the focus on the goals and approaching them efficiently.

My thanks also go out to my supervisors and former colleagues at Montanuniversität Leoben, Nikolaus August Sifferlinger and Eric Fimbinger. Thank you for contributing to this work and granting me an excellent connection to the university.

I also want to thank my parents and my girlfriend for their unconditional support, since without them, my studies would not have been possible at all. Thank you for having my back at all times.

Abstract

Differential settlement along ballasted railway tracks is one of the main factors that force maintenance work. The elasticity of the sleeper (the railroad tie) plays a key role in transferring the wheel-rail contact forces to the ground, and thus, impacts the long-term track settlement due to the occurring local pressure distribution. A deeper physical understanding of the interaction between the railway sleeper and the ballast can help to improve the railway infrastructure and thereby reduce maintenance activities significantly. Due to the discrete nature of railway ballast, the discrete element method (DEM) is considered a suitable and widely used numerical tool to gain insight into the physical phenomena at particle level and to simulate the bulk behaviour of ballast. In recent DEM related railway track research, the sleeper is either modelled as a rigid body, built up by bonded particles or implemented by a complex coupling method. Since sleeper elasticity significantly impacts the dynamic interaction of the sleeper with the ballast bed, efficient DEM simulations with accurate elastic sleeper models are needed. In this thesis a method is presented that uses the particle facet model (PFM) to design an elastically deformable sleeper. The PFM uses nodes, cylinders, and so-called PFacets to construct flexible objects and was initially utilised to model elastic roots, grids, and membranes with a smooth surface. This approach is adapted to replicate a smoothed surface elastic sleeper without the need for coupling techniques. This way, railway track simulations can be carried out that consider the effects of sleeper elasticity on the discrete railway ballast realistically.

DEM simulations in a box-test setup were carried out in which the elastic PFM sleeper was placed on a compacted ballast bed and then cyclically loaded. The computed pressure distribution at the sleeper-ballast interface, the sleeper deflection profile and the settlement were in qualitative agreement with the literature. In contrast to rigid sleeper models and numerical tools that consider the ballast as a continuum, the simulations have shown that the aforementioned results heavily depend on the initial configuration of the ballast bed.

The proposed modelling method offers an realistic integration of elastic sleepers into ballasted railway track DEM simulations and thereby improves the understanding of the physical effects resulting

from the sleeper's elasticity. Numerical studies of complex railway track regions where the sleeper's mechanical properties are decisive, as found in curves or turnouts, are thus made possible.

Kurzfassung

Variierende Fahrwegsetzung entlang von Schottergleisen ist ein entscheidender Grund, dass Instandhaltungsarbeiten durchgeführt werden müssen. Die Elastizität der Bahnschwelle spielt bei der Übertragung der Rad-Schiene Kräfte in den Untergrund eine wichtige Rolle und beeinflusst dadurch das Setzungsverhalten des Schotterbettes aufgrund der sich einstellenden lokalen Druckverteilung. Ein tieferes, physikalisches Verständnis über die Interaktion zwischen Bahnschwelle und Schotter kann dazu beitragen, Verbesserungen am System vorzunehmen und damit den Wartungsaufwand deutlich zu reduzieren. Aufgrund des diskreten Charakters des Gleisschotters gilt die Diskrete Elemente Methode (DEM) als geeigneter und weit verbreiteter numerischer Ansatz, um Einblicke in die physikalischen Phänomene auf Partikelebene zu erlangen und um das Schüttgutverhalten des Schotters zu simulieren. In bisherigen DEM Simulationen des Schienenoberbaus wurde die Schwelle entweder als starrer Körper modelliert, aus Bonded-Particles aufgebaut oder durch komplexe Co-Simulationen implementiert. Da die Schwellenelastizität die dynamische Wechselwirkung zwischen Schwelle und Schotter maßgeblich beeinflusst, sind effiziente DEM-Simulationen mit einer präzisen Abbildung von elastischen Schwellen unerlässlich. In dieser Arbeit wird eine Methode präsentiert, die das Particle Facet Modell (PFM) verwendet, um eine elastisch verformbare Bahnschwelle zu modellieren. Die PFM verwendet so genannte Nodes, Cylinder und PFacets um Objekte aufzubauen und wurde ursprünglich verwendet um elastische Wurzeln, Gitter und Membranen mit glatter Oberfläche darzustellen. Dieses Modell wurde angepasst, um eine elastische Schwelle zu modellieren, ohne auf Co-Simulationen zurückgreifen zu müssen. Dadurch können Simulationen des Bahnoberbaus durchgeführt werden, die die Effekte der Schwellenelastizität auf diskretem Schotter realitätsnahe berücksichtigen.

Es wurden DEM Simulationen von Schotter-Box-Tests durchgeführt, in denen die elastische PFM Schwelle auf einem verdichteten Schotterbett platziert und im Anschluss zyklisch belastet wurde. Die berechnete Druckverteilung an der Schwelle-Schotter Grenzfläche, die Biegelinie der Schwelle und die Fahrwegsetzung stimmen qualitativ mit Daten aus der Literatur überein. Im Gegensatz zu

starren Schwellenmodellen und numerischen Ansätzen, die den Schotter als Kontinuum betrachten, zeigen die Simulationen, dass die zuvor erwähnten Ergebnisse stark von der Ausgangskonfiguration des Schotterbettes abhängen.

Die präsentierte Methode ermöglicht eine realitätsnahe Integration von elastischen Bahnschwellen in DEM-Simulationen des Schotteroberbaus und verbessert dadurch das Verständnis für die durch Schwellenelastizität resultierenden physikalischen Effekte. Numerische Untersuchungen von komplexen Fahrwegsabschnitten, in denen die mechanischen Eigenschaften der Schwelle entscheidend sind, wie in Bögen und im Weichenbereich, können dadurch ermöglicht werden.

Contents

1 Introduction

2021 - it is the second year strongly affected by the CoViD 19 pandemic crisis in central Europe. New mutations are spreading faster than any others before while the economy is scared of further lockdowns. Scientists claim that climate change directly impacts how people live with other species on earth, which drastically influences when and where pathogens appear. To limit the risk and impact of infectious diseases, it is advised to vastly reduce greenhouse gas emissions and thereby the rise of the average global temperature. This can be achieved by reducing air pollution, mainly caused by burning fossil fuels like coal and oil, by making the workforce more climate-resilient through scaling up investments in low-carbon technologies. [1–3]

One of the big concepts to reduce climate change impact is the European Green Deal, which was made public by the European Commission by the end of 2019. The goal is to reduce the net emissions of greenhouse gases to zero and to become the first continent to be climate neutral. When it comes to emissions, the first thing coming into mind are vehicles with combustion engines that should be significantly reduced. Passenger cars alone contribute 15% to the total CO_2 emissions of the EU27, transportation of goods not to mention, and when compared to other transportation types, it is clear that road traffic needs to be reduced and railway traffic needs to be pushed. [4–6]

One of the approaches to push railway traffic is the European Silk Road. It is meant to connect the industrial centres of western Europe with the continent's populous but less developed regions further east. Additionally, 2021 was assigned to be the "European Year of the Rail" to raise awareness on the benefits of rail-bound transport and promote trains as the most environmentally friendly way for passenger and freight transportation. [5, 7, 8]

All these points come to the same conclusion: a lot will be pushed in the railway industry to accomplish climate neutrality for transportation issues in the future. This means that the railway infrastructure needs to be as efficient as never before and resilient enough to take on the challenge of very high

demand.

1.1 The railway industry

A lot of development and investments in the railway industry could be observed over the last years. Many huge projects are ongoing at the time of writing. In Austria alone, three massive railway tunnels are being built. In general, Austria is a central node of Europe's traffic flow due to its geographical location. Currently, four out of nine of the central lines of the trans-European railway transport network go through Austria. This will become even more significant when all planned European lines, e.g. the European Silk Road, are finished and are working at full capacity. [9–14]
Railway operators and suppliers want their vehicles and tracks to become more efficient while reducing maintenance work or even malfunctioning. For that reason, the *Technical University of Graz* (*TU Graz*), *voestalpine AG*, *Austrian's Federal Railways* (*ÖBB*), *Siemens Mobility Austria GmbH* and *Virtual Vehicle Research GmbH* combined their railway competencies and founded the *Research Cluster for Railway Systems (RCRS)* research initiative to increase competitive capabilities even further. The spotlight in this consortium is on rail vehicle technology, rail infrastructure, and rail operations, focusing on synergy potential and digital transformation. The partners want to promote joint research projects to leverage on each other's competencies. Thanks to innovative companies and research institutions, Styria has already made a name in this field over the recent years. Other scientific institutions, domestic companies and rail operators will join this venture in the future to boost Austrian's rail competence even more and accentuate its expertise throughout Europe. [15–22]

1.2 Scope and outline

Part of ongoing research is developing a deeper physical understanding of ballasted railway tracks. The interaction between the central components of rails, sleepers, and the ballast bed in dynamic

load cases is particularly interesting, including the effects of elastic layers between them. In this thesis, numerical discrete element simulations are carried out to gain insight into ballasted railway tracks. The work of Kumar et al. [23] is used as a basis for box-test simulations. This approach is extended in this thesis by developing a method to include an elastic sleeper model in the simulations. Additionally, the size of the simulation box is increased to cover the sleeper length and the affected ballast around it entirely. This way, it is expected to understand the influence of sleeper elasticity on ballast settlement and contact pressure by performing static and cyclic loading. The results are then discussed and compared to laboratory experiments from the literature and results from other numerical railway track models. Moreover, this simulation approach is meant to provide the base for additional simulations to investigate, e.g. the lateral resistance of the track or the situation of long sleepers in turnouts that are loaded asymmetrically and can develop a hanging sleeper situation.

In the first chapter, the basic setup of ballasted railway tracks is described. A literature summary is presented that investigated the effects of sleeper elasticity through experiments and simulations. In the second chapter, possible approaches for modelling elastic objects in a discrete element environment are discussed. The chosen approach is presented and the model's theory is explained in detail. In chapter three, the simulation setup is presented, including the design, modelling and calibration of the sleeper model, the configuration of the box-test and the simulation procedure. The results obtained from simulations are discussed in chapter four. Finally, in the fifth chapter, a summary and an outlook on future research are provided.

1.3 The ballasted railway track

Many different types of track structures exist around the world. The most frequently used type is the ballasted track, also called "classical track" or "conventional track" for that very reason. It consists of a flat framework made of rails and sleepers that is supported on ballast. The ballast bed rests on a sub-

ballast layer, forming the transition layer to the formation or subgrade. Fastenings, rail pads, switches and crossings are also considered part of the track. The construction principles of a classical track structure are shown in figure 1 and figure 2. Significant developments of the superstructure in the last century include: introduction of continuously welded rails, use of concrete sleepers, heavier rail-profiles, innovative elastic fastenings, mechanisation of maintenance, and introduction of advanced measuring equipment and maintenance management systems. [24]

The main advantages of the ballasted track compared to other track types are: [24]

- efficient drainage
- sufficient elasticity
- proper noise damping
- relatively low construction costs and easy maintenance

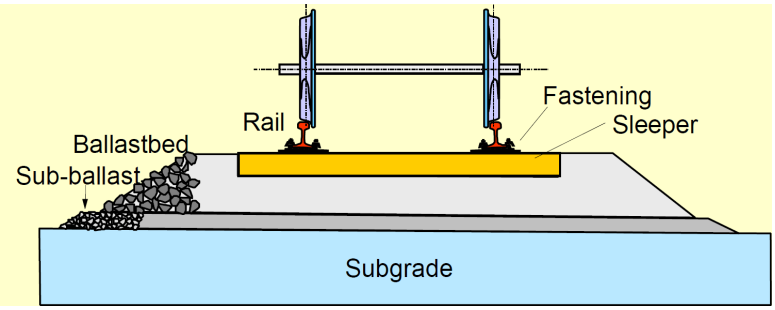

Figure 1: Principal of track structure of a single sleeper section [24]

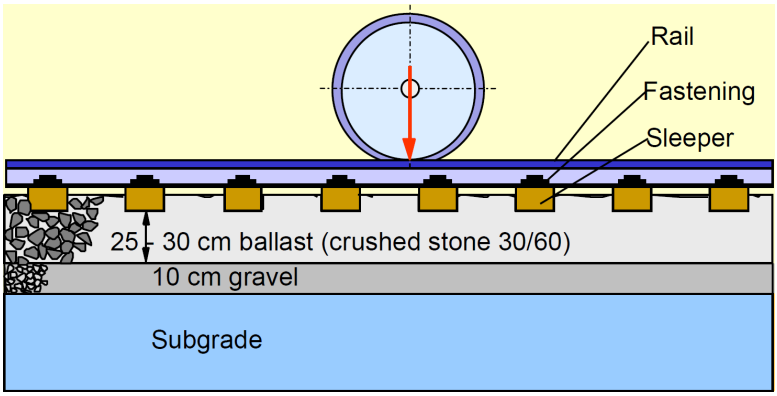

Figure 2: Principal of track structure: longitudinal section [24]

1.3.1 The ballast bed

The ballast bed consists of a layer of loose, coarse-grained material that can absorb considerable compressive stresses due to internal friction between the grains, but not tensile ones. The thickness of the ballast bed is such that the subgrade is loaded as uniformly as possible. The optimum thickness is usually between 25 and 30 cm measured from the bottom of the sleeper. Besides distributing the load evenly, the ballast bed needs to also provide adequate lateral resistance. Moreover, the draining effect of the bed is vital as it must withstand heavy rainfalls without flooding the track. [24, 25]
The primary functions of the ballast bed can be summarised as follows: [25–27]

- transferring and distributing the load from the sleepers to a large area of the formation
- providing elasticity and resilience to the track for proper riding comfort
- providing the necessary resistance and stability in longitudinal and lateral direction
- providing effective drainage to the track
- providing an effective means of maintaining the level and alignment of the track

The ballast material's most essential requirements are hardness, wear resistance, and good particle size distribution. The particles themselves must have sharp edges, which helps in increasing shear resistance. Some of the more commonly used types of ballasts are crushed stone (broken rock like granite, kieselkalk or calcite), gravel (obtained from rivers) or crushed gravel. For special circumstances other types of ballast (e.g. sand or moorum) may also be considered. Ballast between 32 mm and 50 mm should be generally used, but it is recommended to use grain sizes on the upper limit since it will break down in operation. [24, 25]
To summarise, the ballast material should possess the following properties: [24–27]

- adequate toughness, hardness, durability, wear-resistance, and no absorption of water.
- cubical shape with sharp edges

- effective drainage for water
- cheap, economical, and available in large amounts

1.3.2 Sleepers

The transverse ties that are laid to support the rails are called sleepers. Sleepers are the essential elements that transfer the dynamic wheel load from the rails to the subgrade through the ballast bed and need to fulfil the following functions: [24, 25]

- sustain and transfer rail forces as uniformly as possible to the ballast bed
- provide longitudinal and lateral stability
- act as an elastic medium to absorb blows and vibrations
- preserve track gauge and rail inclination

The commonly used types of sleepers are:

(i) Timber sleepers Timber sleepers have a prismatic shape, are roughly 16 cm high, 26 cm wide, and 2.60 m long, making them around 100 kg heavy. Softwood sleepers (pine-wood) have a low compressive strength perpendicular to the wood grain and are used for the regular track. Hardwood sleepers (beech, oak, tropical varieties) are more robust and offer longer service life. The hardwood type is used in switches and crossings where the sleepers are called bearers. Bearers have the same cross-section as regular timber sleepers yet are up to 5.50 m long. [24, 25]

(ii) Steel sleepers Steel sleepers are less used because of problems with insulation, maintenance, the tendency to corrode and a relatively high price. However, steel sleepers offer some strong points such as long service life, high dimensional accuracy and a positive residual value. [24]

(iii) Plastic and composite sleepers In more recent times, composite railroad sleepers manufactured from recycled plastic resins, recycled rubber, or fibre-reinforced foamed urethane (FFU) have gained the attention of infrastructure managers. The novel sleeper type offers a longer service life than wooden sleepers with an expected lifetime of 30 to 80 years, as the used materials are impervious to rot and insect attack. Additionally, composite sleepers generally offer more freedom in design. Aside from the environmental benefits of using recycled material, these sleepers provide more elasticity and better damping than concrete sleepers, decreasing the intensity of vibrations and sound production. [28]

(iv) Concrete sleepers The development and use of concrete sleepers became significant in the last 70 years due to the scarcity of wood, the introduction of the continuous welded rail (CWR) track, and the improvements in concrete technology and prestressing techniques. The advantages of concrete sleepers are: [24, 25]

- long service life and resistance against biological contamination
- great freedom in design and construction
- relatively simple manufacturing with the possibility of prestressing
- heavy weight of about 200 to 300kg

The heavy weight of concrete sleepers is essential for CWR tracks. If not restrained, rails would lengthen in hot weather and shrink in cold weather. To provide this restraint, the rail is prevented from moving in relation to the sleeper using clips and anchors. An effectively compacted ballast bed and heavy sleepers provide the needed conditions to prevent strong rail deformations and, therefore, less maintenance. Concrete sleepers, in general, provide more strength and stability to the track and maintain better gauge, cross-level and alignment. However, concrete is less elastic than wood, which entails that dynamic loads and ballast stresses for a concrete sleeper can be as much as 25% higher

compared to timber sleepers. Furthermore, additional machinery is needed to handle them due to the heavy weight. [24, 25, 29]

To reduce impacts of the hard surface of concrete on the ballast, it became common to use under sleeper pads (USPs). USPs and other elastic layers used in ballasted railway tracks are now explained in detail.

1.3.3 Elastic layers

One of the main problems in rail transportation are vibrations transmitted from the track to the environment, perceived as noise and vibrations. Additionally, due to the insufficient elasticity of the tracks, the maintenance expenses arising from material wear are not neglectable. On the one hand, a stiff track is needed for proper rail alignment, while on the other hand, more elasticity is required to reduce maintenance costs. For that reason, elastic layers became state-of-art in any major railway line. These layers are made up of polyurethane materials and other polymers to provide the needed elasticity at the critical interfaces. Especially at switches, crossings, transition areas, and expansion compensation, elastic layers became indispensable. [30]

For ballasted railway tracks, the following elastic layers are used:

(i) Rail pads These elastic pads are placed directly under the rail base, as seen in figure 3a. Rail pads increase track elasticity and improve load distribution, yielding greater passenger comfort and less wear on the superstructure. [30, 31]

(ii) Under sleeper pads (USP) USPs are directly mounted to the bottom face of the sleeper, as seen in figure 3b, and provide vibration protection, preserve the ballast and lengthen the service life of the track. The pad increases the contact area between the angular ballast and the underside of the sleeper, which reduces contact pressure. Ballast breakdown and track settlement are therefore diminished

significantly. Ballast tamping and screening cycles are lengthened, resulting in life cycle cost savings. [30, 32]

(iii) Under ballast mats (UBM) UBMs are placed below the ballast bed as shown in figure 3c, reduce airborne noise, and provide vibration protection to preserve the ballast. These mats also decrease the magnitude and increase the time duration of impact forces, which substantially reduces ballast breakage. [30, 33, 34]

(a) Rail pad **(b)** Under sleeper pad **(c)** Under ballast mat

Figure 3: Elastic layers in ballasted tracks [35]

Further parts of the track, like fastening systems and the rails themselves, will not be explained in detail here, as this would go beyond the scope of this chapter. Additionally, these parts are of minor importance for the research conducted in this thesis.

1.4 Track and sleeper research

1.4.1 Ballast settlement

Railway tracks need to become more efficient and less intensive in maintenance. One of the main influences that force maintenance activity is ballast bed settlement due to operation. Irregularities along the track result in dynamic responses of the vehicle. The dynamic loads lead to further development of track irregularities caused by ballast rearrangement and deterioration. Ballast settlement

can be broken down into four main mechanisms: ballast rearrangement, edge breakage, wear, and particle breakage. In figure 4, the ballast settlement with loading cycles is presented, comprising of three different phases. Additionally, the contribution of the settlement mechanisms is indicated for the corresponding phases. In phase I, the settlement occurs relatively fast. Ballast rearrangement (compaction and side-wise spreading) and edge breakage dominate in this phase. Particle breakage only happens when a stone is positioned with an unfavourable orientation. In phase II, particle rearrangement decreases as the local voids in the ballast become less common and settlement slows down. Moreover, edge breakage is significantly reduced while wear starts to slowly become more notable. In phase III, the settlement continues at a slow rate and is dominated by the wear of ballast stones. When the differential settlement along the track becomes too high, tamping is required. [23, 36–42]

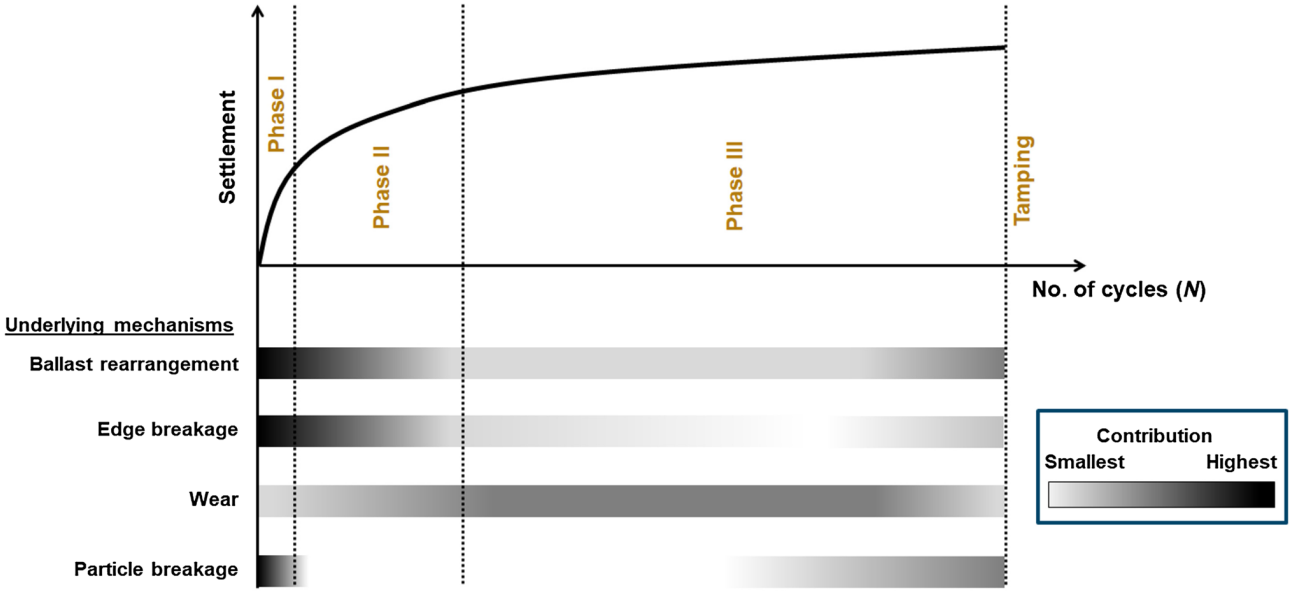

Figure 4: Sketch of sleeper settlement during a ballast tamping cycle [23]

Elastic layers have a significant impact on the sleeper-ballast interface. It was shown that under cyclic loading, USPs reduced the contact stress at the sleeper-ballast interface and had a positive effect on ballast settlement as less settlement was observed. However, the pressure measured at the bottom of

the ballast bed remained unchanged. In terms of UBMs, it was shown that ballast settlement increases with decreasing bottom stiffness under cyclic loading. Higher ballast degradation was observed for the softer UBMs, due to a possible increase in particle movement. [23, 32, 43–45]

1.4.2 Influence of sleeper elasticity

The material stiffness has a significant influence on the settlement behaviour of railway tracks, as discussed in the previous section regarding USPs and UBMs. Different sleeper types with varying material properties are employed in railway tracks. Literature has shown that the properties of the sleeper material influence the track stiffness (deflection) and long-term settlement behaviour. [46]

In laboratory tests, Salih et al. [47] compared different types of sleepers under static loading and observed the sleeper deflection profiles shown in figure 5. On the one hand, sleepers with a low bending stiffness have a prominent W-shaped deflection profile along their length. On the other hand, stiffer sleepers, like prestressed concrete sleepers, show an almost flat profile. Their deflection profile was also captured by a finite element analysis, shown in the right part of figure 5 using the BOEF (beams on elastic foundation [48]) model. The sleeper's bending stiffness greatly contributes to the total track stiffness. Additionally, it was concluded that the sleeper's bending stiffness has more impact on the deflection behaviour, bending moment and shear force of the sleeper than the support modulus of the ballast bed. As Salih et al. [47] has shown, sleepers under static loading can form a pronounced deflection profile; however, considering only static loads might be not sufficient to determine the effects of sleeper bending on track settlement, as realistic loading conditions of passing trains are more complex and are stretched over a longer period. [47, 49]

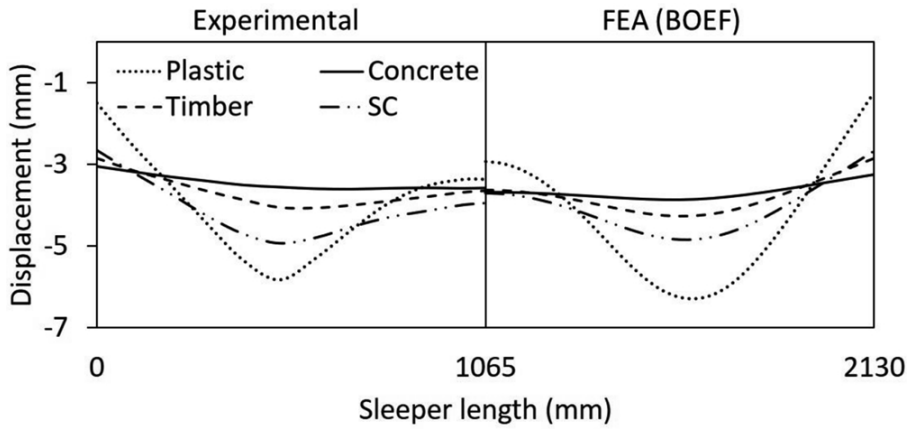

Figure 5: Sleeper deflection shapes. Experimental and finite element analysis [47]

The deflection profiles of various sleeper types subject to multiple load cycles in laboratory experiments were investigated by Ferro et al. [50]. The deflection after ten cycles showed a stiff behaviour for concrete sleepers, while a well-formed W-shape for composite sleepers was observed. Relatively flexible sleepers, in general, apply a less uniform pressure distribution onto the ballast, with higher peaks below the rails. The different distribution of the deflections in the short term (figure 6a) for the composite and concrete sleeper is due to their different flexural rigidity. In the long term, however, a pronounced hogging shape (figure 6b) for the composite sleeper was observed, as substantial gapping between the sleeper ends and the ballast developed because of the increased resilient movement of the sleeper in this region. After three million cycles, the W-shape almost disappeared due to these gaps. In addition, the ballast beneath the sleeper centre became stiffer and denser with loading cycles resulting in reduced settlement in the middle of the sleepers. Therefore, sleeper bending clearly impacts the long-term development of railway tracks as observed in laboratory conditions. [50]

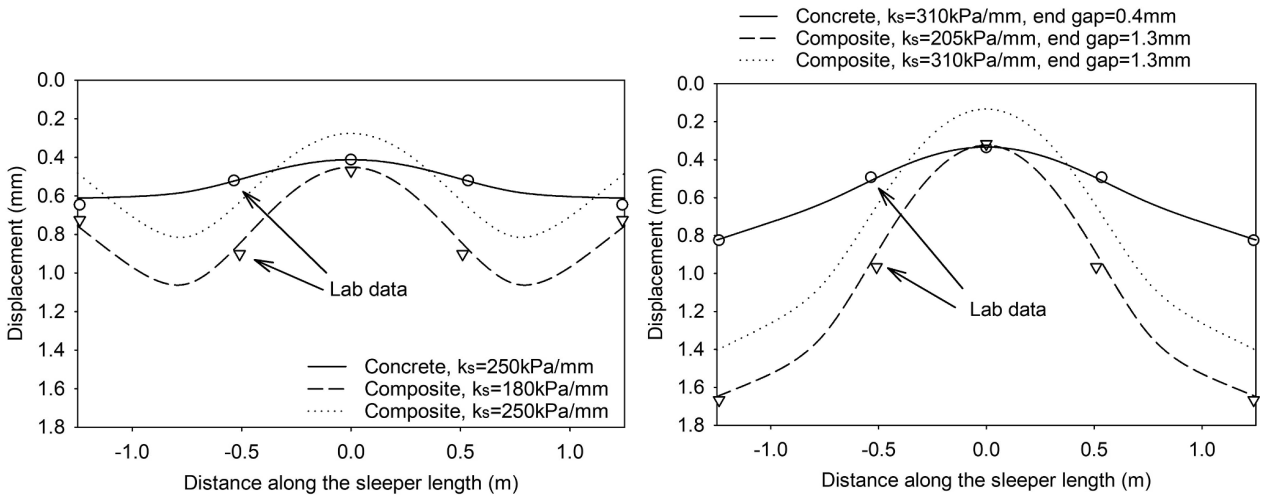

(a) Short-term study **(b)** Long-term study

Figure 6: Sleeper resilient deflection. Laboratory data and BOEF model [50]

The in-service bending behaviour of plastic composite sleepers over several years was studied in the U.S. ([51]) by measuring the maximum downward and upward displacement, which was then compared to the behaviour of timber control sleepers. The results are shown in figure 7. It can be seen that the deflection shapes of the investigated sleeper types are similar but more pronounced for softer (plastic) sleepers, which also depicted more resilient movement of the sleeper ends. This long-term sleeper behaviour is in agreement with the laboratory work of Ferro et al. [50], as previously discussed. Nevertheless, the investigated sleepers in the field tests show an asymmetric deflection profile, which was not depicted in laboratory work. The asymmetry of the deflection profile can be due to several reasons; however, in this case, only little is known about the surroundings of the sleeper, e.g. the ballast, which can significantly influence the deflection profile. [51]

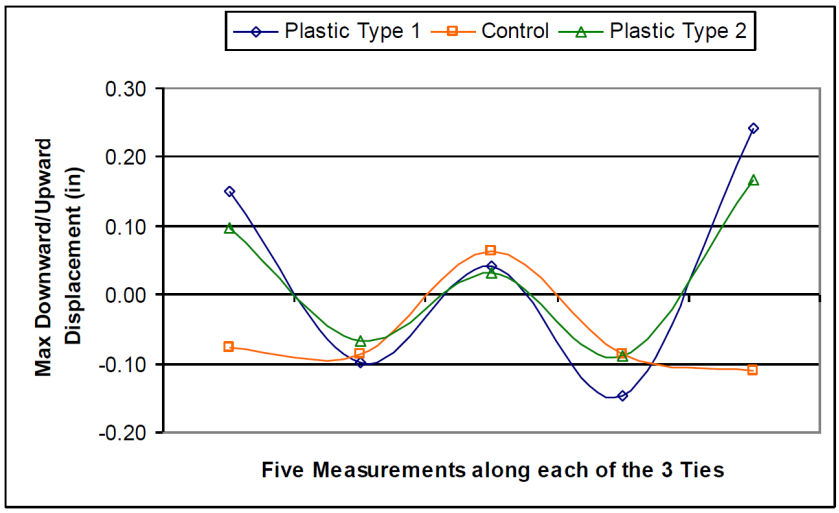

Figure 7: In-service bending shape of various sleeper types (*control* in the legend refers to a timber sleeper) [51]

Railway track behaviour strongly depends on sleeper and ballast properties as prior shown in laboratory experiments; however, it becomes vital in situations where flexible sleepers are installed in rigid surroundings, as Van Belkom [52] points out. In this scenario, the loads on the sleeper can reduce significantly, which decreases the pressure, and the rail deflection can double when sleeper deformation is considered. Moreover, when tracks are not maintained, eventually, gaps between the sleeper and the ballast can occur that close on train passage. These gaps accelerate ballast deterioration and sleeper settlement significantly, and it was shown that the development of these gaps strongly depends on the bending stiffness of the sleeper. All these points mentioned above are clear signs that sleeper bending needs to be considered in future research to gain more insight on how track components interact with each other and how the chosen materials affect railway track behaviour in the short- and long-term perspective. [52]

1.5 Railway track simulations

Laboratory experiments of railway track segments are difficult to set up and require lots of time, space and effort. Additionally, it is complex to measure the physical effects within the ballast bed or at the sleeper-ballast interface. Therefore, numerical simulations became popular as these tools offer quick adaptations and detailed insights. The discrete element method (DEM) is considered an appropriate and commonly used numerical tool to simulate the bulk behaviour of railway ballast due to the discrete nature of the ballast stones, and provides insight into the physical phenomena at the particle level. The prediction quality of DEM simulations depends on three points: the geometrical representation of the single particles, the used contacts models, and parametrisation through principal experiments. For modelling the ballast itself, many different approaches have been used so far. Guo et al. [53] summarised and reviewed known railway ballast models to assist researchers in choosing the appropriate model for specific applications. A few ways to model railway ballast in combination with an (elastic) sleeper model are discussed next. [23, 53–55]

Several DEM works on railway ballast focus on accurate description of particle shape while paying less attention on capturing the underlying physics at the particle scale. Suhr et al. [54, 55] used a balanced approach where a clump particle of three spheres and the conical damage model (CDM, an extension of the Hertz-Mindlin contact model) are used to represent railway ballast. Particle edge breakage and yielding are captured in this approach. A single set of parameters is able to describe the behaviour observed in different experiments. This approach offers computationally efficient simulations with proper bulk behaviour for railway ballast. Kumar et al. [23] used this parametrised model to perform cyclic loading in a box-test for investigating the influence of elastic layers in railway tracks numerically. This approach offered deeper insights into the physical mechanisms at the sleeper-ballast interface and inside the ballast bed. However, the sleeper was modelled as a rigid body that was allowed to move only vertically. Additionally, only a small track segment was covered in the

simulations. [23, 54, 55]

Gao et al. [56] proposed a method that uses bonded sphere clusters as a ballast representation and a sleeper built up of a sphere clump. The difference being that a bonded cluster can break up when a specific stress is reached, while a clump will always stay connected regardless of the stress state. By building up the sleeper through particle clumps, it is possible to adequately represent the geometry of the sleeper. However, this sleeper model will always show a geometrically rough surface and is not able to replicate elastic behaviour. Both of these aspects are crucial for a precise sleeper representation in railway track simulations. [56]

Nishiura et al. [57] tried a novel approach by using the so-called quadruple discrete element method (QDEM) to model the ballast and the sleeper. The QDEM concept uses a four-particle interaction model to replicate the real three-dimensional linear visco-elasticity of bulk material. The QDEM elements were used to model the sleeper in the ballast bed and enabled the computation of its viscoelastic deformation. Hence, this sleeper model can be seen as an extension to the previously mentioned sphere clump sleeper model that additionally covers sleeper bending. In addition to that, many particles need to be used for these simulations, and the discrete timestep drops significantly. To determine sleeper settlement over several loading cycles this approach might be too computationally expensive and the effects of a rough surface persist. [57]

To include a sleeper model with a smooth surface in DEM simulations, Guo et al. [58] replicated the sleeper by a complex wall geometry. This way, the exact sleeper geometry can be considered and the sleeper-ballast contacts can be accurately handled. However, wall geometries in DEM simulations cannot elastically deform, and thus, sleeper bending is not covered in this approach. [58]

To extend the exact sleeper replication with elastic behaviour, Song et al. [59] utilised an open-source DEM-FEM surface coupling method to model elastic sleeper behaviour. Via this coupling method, it was possible to consider sleeper bending and thus evaluate its effects on the pressure distribution

at the sleeper-ballast interface. The sleeper settlement could not reflect the field situation because of more conservative boundary conditions and the use of spherical particles. However, this coupling method shows a valid approach to combine discrete methods with continuum ones to model flexible sleepers in railway tracks. Extension on ballast representation and calibration is needed for proper evaluation. [59]

Most approaches in recent literature tend to use sphere clumps to accurately model ballast stones with either a linear or Hertz-Mindlin contact model. Several similar approaches were found in the literature and are herewith mentioned [60–71]. However, it is possible to model ballast with the same accuracy using a simpler geometrical approach and a modified contact law as was shown in [53–55, 72].

For modelling the sleeper, only a few studies used a complex model to include the deflection of the sleeper within their simulation [57, 59]. However, it is expected that sleeper deformation has a significant influence on ballast behaviour [52]. As mentioned above, these elastic sleeper approaches tend to have several drawbacks and seem computationally expensive. A simple model to include sleeper elasticity in DEM simulations of railway tracks would be of high value, which is, in fact, the focus of this thesis. In the following chapters, a novel approach for elastic sleeper modelling is explained in detail.

2 The approach

2.1 Possible approaches for elastic sleepers in DEM simulations

Multiple different approaches to include deformable objects, like elastic sleepers, in a discrete element method (DEM) environment exist. In this section, some approaches are discussed.

2.1.1 Finite element method (FEM) coupling

When thinking about simulating elastically deformable objects, the FEM has proven to be a suitable choice. The FEM in engineering is primarily used to investigate stress development in geometrically complex structures when analytical solutions are not practical or even possible anymore. However, coupling DEM and FEM to analyse railway ballast and sleeper deformation simultaneously is challenging since a continuum approach (FEM) meets a discrete approach (DEM). Stransky et al. [73] developed an open-source FEM-DEM coupling in the DEM environment of *Yade* [74] and the FEM software *OOFEM* [75]. The surface coupling of this work was later used by Song et al. [59] to investigate sleeper-ballast interactions, as explained in section 1.5.

One of the issues that remain is that coupling methods tend to be relatively slow in terms of computation since two simulations, that depend on each other's input, run simultaneously. Moreover, accurately defining the contact behaviour between the discrete elements and finite elements for a complex three-dimensional object is not a trivial task, and developing a proper interface for the ongoing data transfer between the environments is challenging. [76]

2.1.2 The bonded-particle model (BPM)

To account for the complexity, due to coupling between different tools (FEM and DEM), models were developed that used connected discrete particles within the DEM environment to resemble deformable

objects.

One of these approaches is the bonded-particle model (BPM). The BPM is an additional algorithm turning the pure unbounded DEM into a model capable of replicating the mechanics of continua. An additional interaction model is defined between particles that connects them. This virtually created bond is allowed to have elastic properties and is able to break when a certain stress level is reached. This way, a simple body can be assembled to form an elastic cantilever beam, as shown in figure 8. Even particles of complex shape, as Fimbinger [77] proposed, can be bonded to build up fully flexible objects like conveyor belts. [77–83]

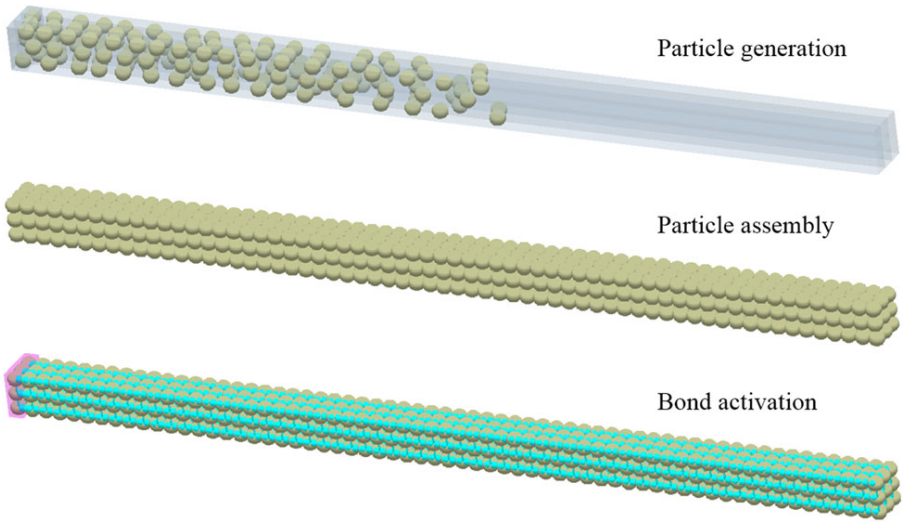

Figure 8: Generation of a cantilever beam model using the bonded approach in DEM [83]

The BPM, therefore, is a possible approach to model elastic sleepers in a DEM environment. However, when spherical particles are used, it is not possible to model an accurate surface. Complex-shaped particles can resolve this issue but are computationally demanding and tricky in terms of implementing the correct behaviour at the contact level [77].

2.1.3 The particle facet model (PFM)

Chareyre et al. [84] proposed a model for implementing elastic objects in the DEM environment using cylindrical connections between spherical particles. Contrary to the BPM, where the bonds are only virtual, the cylindrical connections can also interact with external particles. This way, flexible strings were used to replicate soil reinforcement by plant roots and also wire-meshes or geogrids, shown in figure 9 and figure 10a, respectively. [76, 84–90]

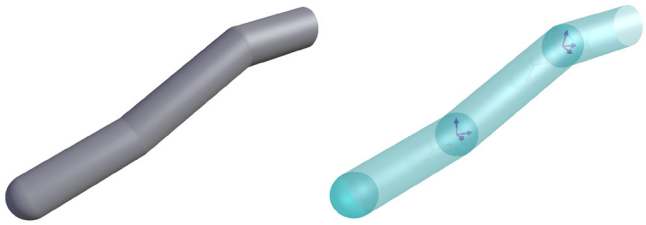

Figure 9: DEM plant roots [85]

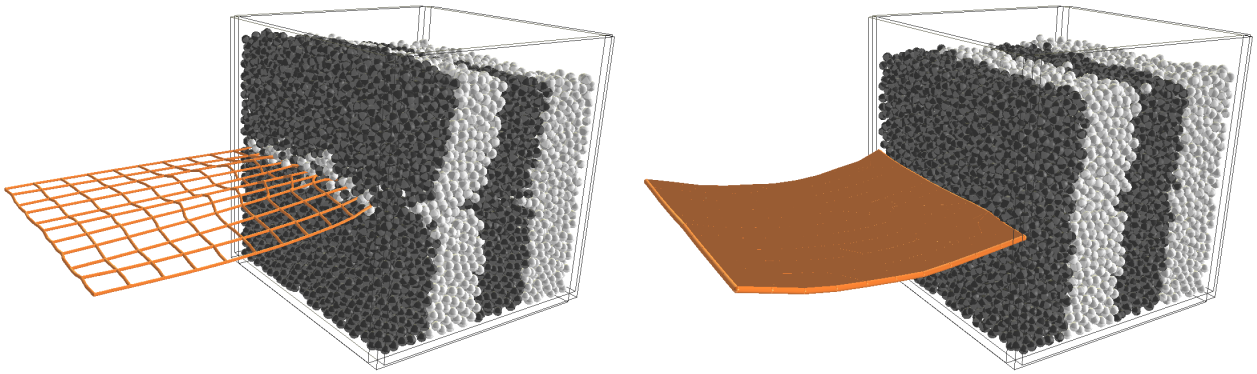

(a) DEM geogrid **(b)** DEM membrane

Figure 10: DEM geogrid and membrane comparison [76]

Effeindzourou et al. [76, 88–90] extended the cylindrical model with so-called particle facets (PFacets) to extend the approach to also cover smooth membranes. Three nodes, each connected via cylindrical connections, build up a triangle that is then covered with two facets. Several triangular PFacets can then share corner nodes to form membranes or three-dimensional shell bodies shown in figure 10b

and figure 11, respectively. This approach basically combines a simple bonded-particle model and adds additional surfaces for proper contact management. [76, 88–90]

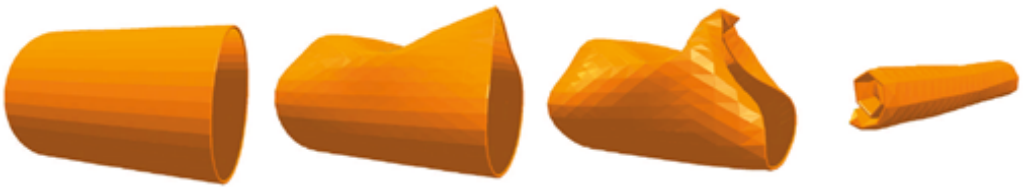

Figure 11: Deformable three-dimensional DEM shell body [88]

2.1.4 The chosen modelling approach

Each of these methods and models mentioned above has its strengths and drawbacks. In this work, it was decided to use the PFM approach from Effeindzourou et al. [76, 88–90] due to the following reasons:

- smooth surface modelling
- no coupling needed (and therefore less effort)
- available as open-source in *Yade*, including examples
- documented, tested, and explained in several papers
- no complex-shaped particles needed

Additionally, the goal of this research is to use the calibrated ballast model of Suhr et al. [54, 55] and the box-test setup used by Kumar et al. [23]. Both studies were conducted in *Yade* and, since the approach using particle facets was also introduced within the same framework, efficient modelling and fast simulations are expected using the PFM approach.

2.2 The PFM approach

2.2.1 General structure

The discrete element method (DEM) models assemblies of locally deformable particles that interact by contact forces [91]. The interaction between each particle is defined via a contact model. The motion of the particles are computed by Newton's second law using an explicit time-stepping algorithm. For each time step the contacts are updated and the corresponding contact forces are applied on the particles. During the simulation procedure, the particles are allowed to overlap and the resulting contact forces are defined as a function of these overlaps. [76, 88–91]
For implementing the elastic bodies using the PFM, three different types of DEM bodies are needed:

(i) Node elements Nodes are the core bodies of this model that are typically geometrically represented by spheres and responsible for the elastic behaviour of the object, explained in detail in section 2.2.2. In *Yade* a node element is further referred to as a *GridNode*. [76, 85, 88–90]

(ii) Cylinder elements Cylinders (or cylindrical connections) are defined between two nodes. These cylinder elements are geometrically constructed by the Minkowski sum of a sphere and a segment. Hence, compared to a bonded-particle model consisting of a row of multiple spheres, it does not show any numerical roughness. The basic design of a cylinder and a comparison to the bonded-particle model is shown in figure 12. It is worth noting that one node can be part of many cylinders, which offers the possibility to build up one- or two-dimensional structures, such as grids. A cylinder element is further termed *GridConnection* in *Yade*. [76, 85, 88–90]

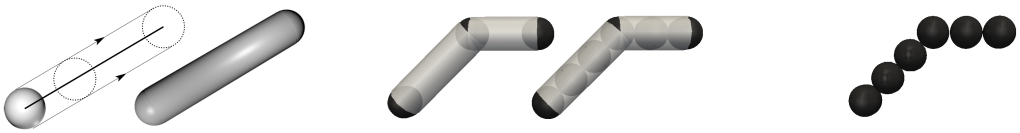

(a) Single cylinder [89] **(b)** Interconnected cylinder [76] **(c)** Bonded cylinder [76]

Figure 12: Discretisation of a cylinder element

(iii) Particle facets Particle facets (termed PFacets) are extending elements introduced to model arbitrary deformable objects. PFacets geometrically correspond to the Minkowski sum of a triangular facet and a sphere, and are composed of three nodes, three cylinders, and two facets. The geometrical construction and composition are demonstrated in figure 13. As can be seen, this approach offers the modelling of smooth surfaces, and as mentioned before, nodes can be part of multiple cylinders, which is also valid for PFacets. [76, 88–90]

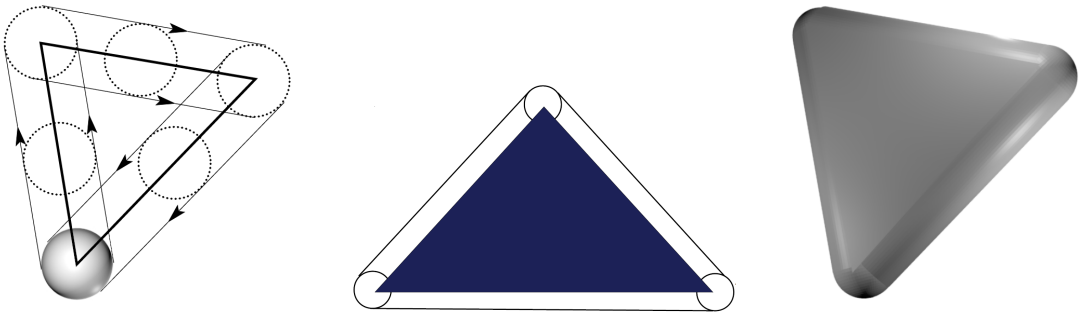

(a) PFacet creation [89] **(b)** PFacet composition [88] **(c)** Final PFacet shape [89]

Figure 13: The PFacet element

All these elements work together to build up elastic objects. However, in order to understand how the interactions between the elements are computed within the simulation framework, it is necessary to separate internal and external mechanics. Internal mechanics cover the behaviour of the elastic object subject to forces, while external mechanics cover the situation of external particles getting into contact with the object.

2.2.2 Internal mechanics

The elasticity of a body modelled by the PFM depends solely on the interactions between nodes. Connections and PFacets do not contribute to the internal mechanics and only follow the movements of the nodes. Hence, an increase or decrease in volume (and corresponding surface) can appear. Additionally, the body's mass is lumped into the nodes, meaning that the mass is discretised. [76, 85, 88–90]

Nodes are assigned a cohesive material (*CohFrictMat*) in *Yade*, and specific values for normal and shear cohesion need to be defined. These two parameters are needed to maintain the interactions between nodes and to define the elastic limits. If the values of the cohesion parameters are exceeded, the interaction is lost. This interaction loss can be viewed as plastic material behaviour. If only elastic behaviour is wanted, the values for cohesion should therefore be set adequately high. Furthermore, the interaction between nodes is only virtual and is not geometrically represented in the simulation framework. [76, 85, 88–90]

Once an interaction between two nodes is defined, their initial distance L_c, the node radius R_c, the Young's modulus E and the shear modulus G are used to compute the stiffnesses of each possible displacement as visualised in figure 14. These stiffnesses are used to compute repulsive forces and torques via a linear spring model when changes in the relative position are detected. The four cases of displacement that can occur between nodes and the mathematical computation of the corresponding stiffness and repulsive force/torque are explained in the following. The equations originated from identifying the classical beam stiffness matrix used in the FEM with the classical elementary stiffness matrix. Details are explained by Bourrier et al. [85]

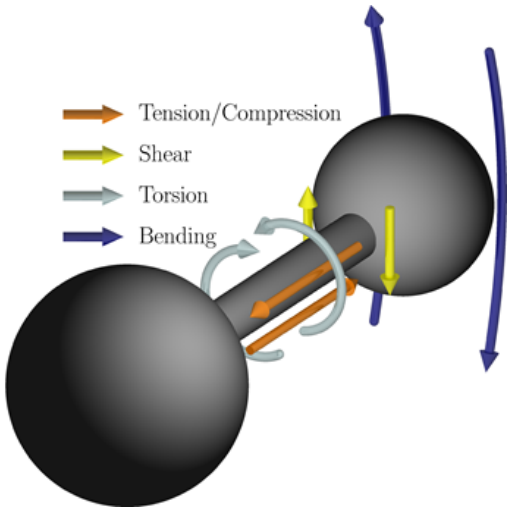

Figure 14: Possible deformation of two interacting nodes [92]

(i) Normal deformation The equations for computing the stiffness k_n and force F_n for elongation/compression are given in equation 1 and equation 2, respectively. The corresponding sketch can be seen in figure 15, where ΔL is the elongation of the node distance. [85]

$$k_n = \frac{E \cdot (\pi \cdot R_c^2)}{L_c} \quad (1)$$

$$F_n = k_n \cdot \Delta L \quad (2)$$

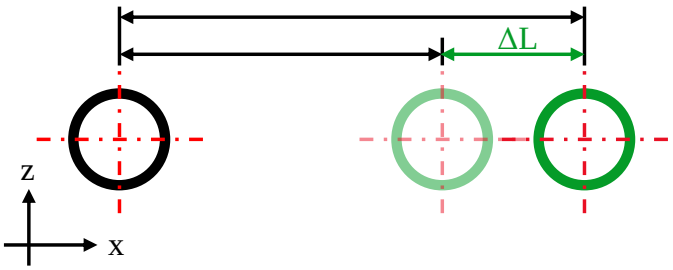

Figure 15: Sketch for elongation or compression

(ii) Shear deformation The equations for computing the stiffness k_s and force F_s for shear deformation are given in equation 3 and equation 4, respectively. The corresponding sketch can be seen in figure 16, where ΔS is the shear distance. [85]

$$k_s = \frac{12 \cdot E \cdot}{L_c^3} \cdot \frac{\pi \cdot R_c^4}{4} \quad (3)$$

$$F_s = k_s \cdot \Delta S \quad (4)$$

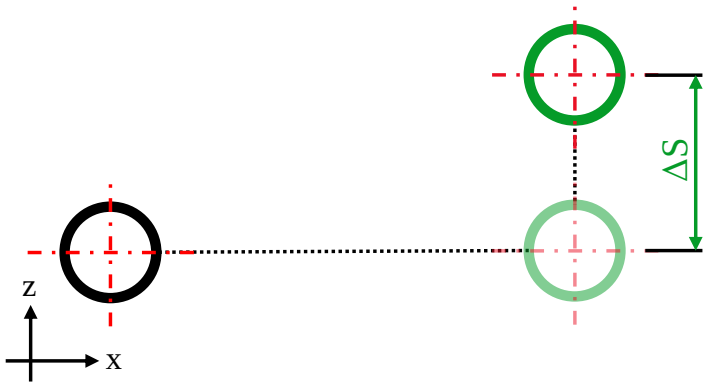

Figure 16: Sketch for shear deformation

(iii) Rotational deformation The equations for computing the stiffness k_r and force F_r for rotational deformation are given in equation 5 and equation 6, respectively. The corresponding sketch can be seen in figure 17, where β is the rotation angle. [85]

$$k_r = \frac{E}{L_c} \cdot \frac{\pi \cdot R_c^4}{4} \quad (5)$$

$$M_r = k_r \cdot \beta \quad (6)$$

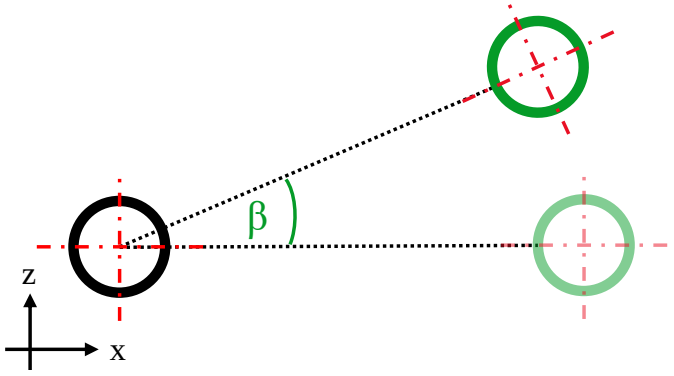

Figure 17: Sketch for rotational deformation

(iv) Twisting deformation The equations for computing the stiffness k_{tw} and force F_{tw} for twisting deformation are given in equation 5 and equation 6, respectively. The corresponding sketch can be seen in figure 18, where γ is the twisting angle. [85]

$$k_{tw} = \frac{G}{L_c} \cdot \frac{\pi \cdot R_c^4}{2} \tag{7}$$

$$M_{tw} = k_{tw} \cdot \gamma \tag{8}$$

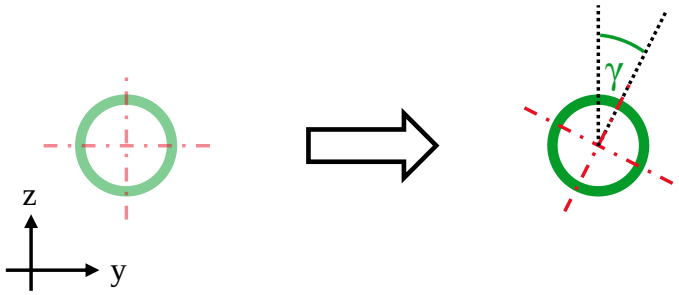

Figure 18: Sketch for twisting deformation

2.2.3 External mechanics

Connections and PFacets deal with contacts between the elastic body and DEM particles and, therefore, different material properties can be defined for these elements to describe the interaction with external particles. Using two different materials for internal and external mechanic computations makes it possible to manipulate each behaviour separately. The basic principles for contact and contact point computation are thoroughly explained by Effeindzourou et al. [76, 88–90].

At the contact point of an external particle with a cylinder or PFacet, a virtual sphere is introduced within the element to take over the contact computation. This virtual sphere has the same radius as the nodes and cylinders. Introducing this virtual sphere makes it possible to manage the contact as a typical sphere-sphere DEM contact as visualised in figure 19a and figure 20, where S is a spherical particle and S_C is the virtual sphere of the cylinder. The resulting forces of the contact are interpolated and distributed to the connected nodes. This contact management also allows contact handling between different PFM elements. Illustrated in figure 19b, two virtual spheres S_{C_1} and S_{C_2} are used to manage the contact between two cylinders that do not share nodes. [76, 88–90]

(a) Sphere-cylinder contact **(b)** Cylinder-cylinder contact

Figure 19: Application of the virtual sphere [90]

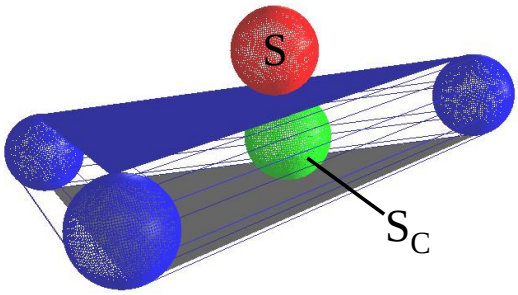

Figure 20: Sphere-PFacet contact [89].

Contacts at edges, corners or intersections are especially crucial for this model since multiple contacts between the elastic body and an external particle can be detected (element overlap) and have to be treated differently. In figure 21, two situations are shown. Indicated by the red and yellow lines, it can be seen that a different amount of contacts needs to be considered for the two shown situations. Details on multi-contacts are thoroughly explained by Effeindzourou et al. [76, 88–90].

(a) Convex configuration **(b)** Concave configuration

Figure 21: Contact between a sphere and two PFacets [90]

The PFM includes these conditions to cover for the transition from one element to another. For newly detected contacts inside an element, a search is conducted to determine whether the contact has moved on from an neighbouring element. If an old contact is found, the contacts parameters are transferred and used to compute the new contact forces. As demonstrated by the plot in figure 22, it can be seen that for three connected and fixed cylinders C_1, C_2 and C_3, the contact force of a sphere sliding over the cylinders stays constant. The same conditions are considered for PFacets and enable a smooth transition from one PFacet to another. [76, 88–90]

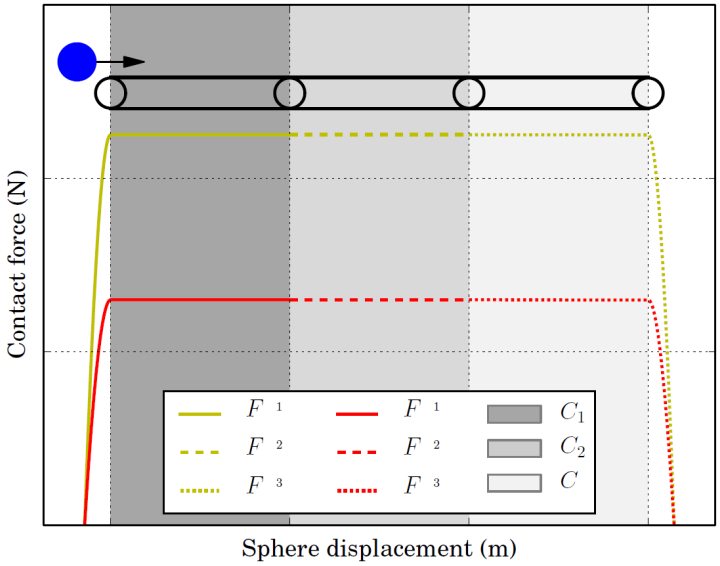

Figure 22: Contact forces for a sphere moving along three fixed cylinders [76]

3 The box-test

This chapter covers the modelling method used in this work to build an efficient railway track DEM simulation setup replicating a box-test. The simulation setup represents one sleeper section of a regular straight track. The box-test simulation consists of the box itself, the railway ballast, and a sleeper. The whole simulation setup is designed to enable easy and fast adaptations and extensions for future work. Each component of the box-test and its modelling approach will be thoroughly explained next.

3.1 The box

The work of this thesis extends the box-test simulations carried out by Kumar et al. [23]. Increased box dimensions are needed to cover all effects accurately that sleeper elasticity might induce. Therefore, the used box is 3.5 m in length and 1.0 m in width. The height of the ballast bed remains at 0.3 m. This way, the full sleeper and an adequate amount of surrounding ballast are represented. With these box dimensions, the ballast volume increases by 14 times compared to the box dimension used in Kumar et al. [23]. The material parameters for the box are chosen to represent steel and were taken from Kumar et al. [23]. The dimensions of the previous work and the work conducted in this thesis are summarised in table 1. The box was modelled using a *FrictMat* material in *Yade* [74]. The assigned material parameters are presented in table 1.

	Kumar et al. [23]	Values in the present work
Young's modulus	200 [GPa]	
Density	7834 [kg/m^3]	
Poisson's ratio	0.28 [-]	
Coulomb's friction coefficient	0.2 [-]	
Box length	0.5 [m]	3.5 [m]
Box width	0.5 [m]	1.0 [m]
Filling height	0.3 [m]	0.3 [m]
Box volume	0.075 [m^3]	1.05 [m^3]

Table 1: Material parameters and dimensions of the box-test setup

3.2 Ballast modelling

3.2.1 Geometrical representation

Several approaches to model railway ballast within a discrete element method (DEM) framework exist, as discussed in section 2.1. Kumar et al. [23] used the railway ballast model of Suhr et al. [55], where the ballast shape is represented by a sphere clump consisting of three non-overlapping spheres of different radii, as shown in figure 23. In the work of Kumar et al. [23], the size of the initially calibrated particles from Suhr et al. [55] was changed to fit the ballast stone's d_{50} size ([24]) and to reduce simulation time. A similar approach is considered in this work. The aforementioned increased box size entails that more particles are needed for the simulations. Since the number of particles amplifies the simulation time drastically, the ballast particles are rescaled in this work. The clump particle's major axis (demonstrated in figure 23) is scaled by a factor of 1.8 in terms of allowing efficient simulations. The final particle dimensions, together with a comparison to the previous representations, are given in table 2. [23, 55]

	Suhr et al. [55]	Kumar et al. [23]	Dimensions of the present work
Major axis	25.6	40	72
Radius R_1	7	10.9375	19.6875
Radius R_2	5.8	9.0625	16.3125
Radius R_3	5	7.8125	14.0625

Table 2: The particle dimensions used in the present work together with a comparison to the previous representations. All dimensions in millimetres.

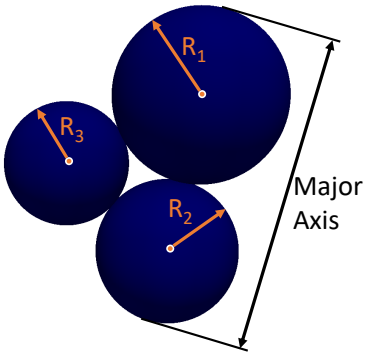

Figure 23: The sphere clump representing a ballast stone

3.2.2 The contact model

Kumar et al. [23] used the conical damage model (CDM) to compute the interaction forces in the simulations. This model was initially proposed by Harkness et al. [93] and adapted for railway ballast by Suhr et al. [54, 55], including proper DEM contact model calibration conducted by compression and direct shear experiments in a box-test. The CDM is based on the non-linear Hertz-Mindlin contact law. When the contact stress in the normal direction exceeds a specific limit, ideal plasticity is introduced to replicate edge breakage of the ballast. In the tangential direction, the Hertz-Mindlin law remains unchanged. [23, 54, 55, 93]

The initial goal of this thesis was to use the CDM for the simulations. However, the particle facet model (PFM) in *Yade* is a complex approach and only supports the linear spring contact model at the

time of writing. Therefore, the simpler linear contact model is used here to model all interactions and to present a method that accounts for sleeper elasticity (and thus the more-complex CDM is neither used for the ballast nor for the sleeper for now). The material parameters for kieselkalk (taken from Kumar et al. [23]) were used for the contact model and are presented in table 3. Though the ballast interaction is only modelled by the linear contact model, the parameter values taken are not entirely off and are expected to describe qualitative behaviour. Additionally, by missing out on the plasticity component (edge breakage) of the CDM, it can be said that only the influence of ballast rearrangement is contributing to the sleeper settlement behaviour.

Young's modulus	30 [GPa]
Density	2660 [kg/m^3]
Poisson's ratio	0.2 [-]
Coulomb's friction coefficient	0.45 [-]

Table 3: DEM material parameters used for the linear contact model for ballast

3.3 Sleeper modelling

3.3.1 Geometrical modelling and implementation

The particle facet model (PFM) is used to design the elastic sleeper, as mentioned in section 2.1.4. A prismatic shape is chosen for simplicity to ensure model stability and to be able to evaluate and validate its mechanical behaviour. Timber sleepers also have a prismatic shape and reduced elasticity compared to concrete sleepers, which leads to a clear W-shaped deflection profile [50]. Therefore, a timber sleeper is chosen here to verify the modelling approach as the deflection results are suspected to be more pronounced. The properties of the timber sleeper used in this work are presented in table 4.

Length	2.60 [m]
Width	0.26 [m]
Height	0.16 [m]
Young's modulus	13.82 [GPa]
Poisson's ratio	0.167 [-]
Density	690 [kg/m^3]
Weight	74.63 [kg]

Table 4: Timber sleeper properties considered in this work

The sleeper geometry is designed in the open-source software *Gmsh* [94]. *Gmsh* additionally offers the possibility to mesh an object like commonly done in the preprocessing of finite element simulations. After meshing the model's surface, it is possible to export all vertices and connecting elements into a *mesh* file that can then be directly imported into *Yade* to build the designed object out of PFM elements. The sleeper mesh has 124 nodes (31 along the sleeper edges), 366 cylindrical connections and 244 PFacets. Therefore, the sleeper model is made up of 734 discrete elements. The sleeper after meshing is shown in figure 24 and is made to be symmetric about the centre plane.

In addition to the positions and connections given by the mesh, a radius for the node elements, and therefore also for the cylinders and PFacets, is required. This radius is chosen to be 6 mm, which seems appropriate as it is significantly smaller than the sleeper's dimension, as well as smaller than the smallest particle radius present in the simulations. This way, the influence of sleeper edges and corner roundings can be considered neglectable. It should be noted that the PFM radius should not be set too small as it slows down simulation speed.

Only the required elements should be implemented to keep the model simple and efficient. Therefore, a shell structure of the sleeper is considered, meaning that the sleeper model is hollow inside. The node elements are only placed on the edges of the sleeper model to provide a stable shell. This approach is considered feasible, as the primary deformation of a sleeper is bending, which can be represented adequately by this chosen shell structure.

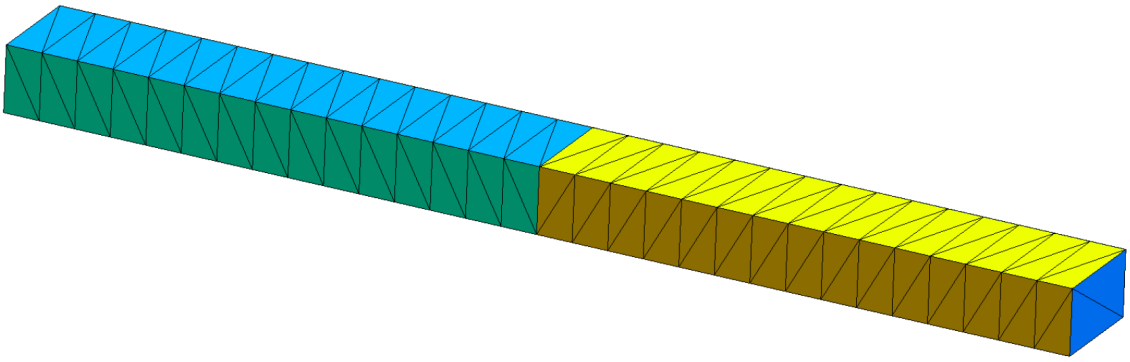

Figure 24: The sleeper design and applied mesh in *Gmsh* [94]. Colours are used to show the symmetric meshing of the sleeper.

Side note: The initial design of the sleeper model considered a shell structure with additional nodes within the faces of the sleeper for a higher resolution in the transverse direction of the sleeper. However, this concept has shown a collapse of the sleeper faces because the hollow model is missing an inner support structure for the nodes within a sleeper face. The aforementioned design was introduced to avoid unwanted deformations and to provide proper stiffness to the model.

3.3.2 DEM internal model parameters for the sleeper

In this section, the adaptation of the parameters for the sleeper model to be used for the simulations is discussed.

(i) Density Since a shell representation is considered for the sleeper in the DEM the mass computation within the DEM model needs to be adjusted. The mass in the PFM to model an elastic sleeper is lumped into the nodes, as mentioned in section 2.2.2, which means that the density of the node material needs to be adjusted to ensure the accurate total weight of the sleeper. The nodes are assigned a density ρ_{new}, different than the sleeper density, to ensure that the correct sleeper mass is achieved in simulations. The density of the nodes is given in table 5, which leads to the desired sleeper weight of 74.63 kg. The discretised mass distribution is thought to not show influence on sleeper oscillations

as the frequencies used in this work (3 Hz) are much lower than the first natural frequency of wooden sleepers (at approximately 61.77 Hz) [95].

(ii) Young's modulus The various stiffness components are computed using the node radius, as explained in section 2.2.2. However, for a complex structure, like the used sleeper model in the simulation, these stiffness components are to be adapted to describe the correct bending behaviour of the physical sleeper. In *Yade*, each stiffness is initially defined when an interaction is established and can be changed later. Here, after the density calibration of the node element, the corresponding Young's modulus is adjusted to achieve proper bending behaviour.

In contrast to density adjustment, it is not straightforward to determine a corresponding factor for the Young's modulus as the sleeper model has a complex structure, and multiple different spring components are active simultaneously in a rather complex arrangement. Since the primary deformation considered here is sleeper bending, the deformation of a cantilever beam subject to a single load at the very end was considered for the calibration of the Young's modulus to achieve the same bending behaviour in simulations as for the physical sleeper. A sketch of the situation is given in figure 25. The assumption is made here that the PFM beam behaves like an Euler-Bernoulli beam. This comparison is only valid when the beam's length L is significantly higher than its cross-sectional dimensions and the beam's deflection is significantly smaller than the length of the beam. To meet these requirements, the cantilever beam used for calibration is three times longer than the sleeper model (7.8 m in total) and the applied load F is set to 2500 N. In equation 9 and equation 10, the analytic deflection computation for a rectangular cross-section with width W and height H is shown. The final Young's modulus is given in table 5. It should be noted that this way of calibration is only valid for bending and that the calibrated parameters are mesh-design- and node-radius-specific. To ensure only elastic deformation, the cohesion parameters of the node material were set adequately high, as presented in table 5. A detailed explanation of these two parameters is given in section 2.2.2.

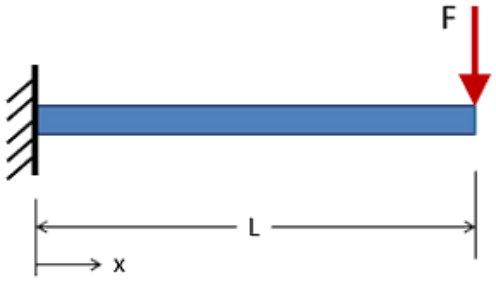

Figure 25: Sketch of a cantilever beam subject to a point load F [96]

$$I = \frac{1}{12} \cdot W \cdot H^3 \qquad (9)$$

$$\delta_{\text{end}} = \frac{F \cdot L^3}{3 \cdot E_{\text{real}} \cdot I} \qquad (10)$$

I ... Area moment of inertia [m^4]

δ_{end} ... Sleeper end deflection [m]

E_{real} ... Young's modulus of the real sleeper [Pa]

Final density	10245 [kg/m^3]
Final Young's modulus	424 [GPa]
Normal cohesion	10^{99} [Pa]
Shear cohesion	10^{99} [Pa]

Table 5: DEM internal material parameters for the wooden sleeper after calibration

In order to test the mechanical behaviour of the cantilever beam, two additional tests were conducted. The first test investigated if the resolution of the beam, precisely the number of PFM elements used to model the beam, has an impact on the deflection using the same set of calibrated simulation parameters. Besides deviations for coarser meshes, the deflection remains consistent for all resolutions, and thus, the chosen mesh resolution was sufficient. The second test examined whether the deflection at each individual node along the beam fits the analytic expectation. In the calibration process, only the deflection at the endpoint was considered. Almost perfect accordance of the node deflection with the analytic deflection profile was observed. These two tests confirm that the introduced calibration

of the sleeper model is done correctly.

3.3.3 DEM parameters for the sleeper-ballast interaction

The material parameters given in table 6 are used to compute interactions between sleepers and ballast particles and are assigned to PFacets and cylinders. The Young's modulus differs from the original internal parameters of a wooden sleeper as the value is taken from Kumar et al. [23] for concrete sleepers interacting with ballast. Values for wooden sleepers are not available yet.

In this work, the external contacts between the sleeper and the ballast are handled by introducing a virtual sphere with the same radius (6 mm) that was initially defined for the nodes and used for cylinder and PFacet construction. The contact between the virtual sphere (radius of 6 mm) and an external particle is not entirely accurate for a contact on a sleeper surface. For a more precise contact computation, the radius of the virtual sphere used to compute the interactions needs to be set to a much higher value while keeping the geometrical radius of the PFM elements unchanged. This way, such a contact would be represented as a proper wall-particle contact. The manipulation of the contact computation, including a detailed calibration, should be conducted in future work.

Yade material type	*FrictMat*
Young's modulus	51.409 [GPa]
Poisson's ratio	0.167 [-]
Coulomb's friction coefficient	0.7 [-]

Table 6: DEM external material parameters for the wooden sleeper

3.4 Simulation procedure

The section covers the individual steps needed to prepare a compacted ballast bed with the right porosity on which a sleeper is first placed and then loaded. The whole simulation process was split into four scripts for easier use and customisation, each accounting for a specific phase. These simulation

phases are discussed in detail in the following sections.

3.4.1 First phase - rainfall

After the box walls and the particle clumps are defined, a virtual volume gets randomly filled with particle clumps. This volume resembles a cuboid covering the whole ground area of the box and has a height of 2 m. The ballast material in this phase has a reduced Young's modulus and a friction coefficient close to zero. This way, a compact ballast bed can be achieved. The ballast particles then set at the bottom of the box due to gravity. As soon as the particles have settled and kinematic energy drops to zero, the bottom wall of the box is vibrated. The bottom plate performs two vibration cycles with an amplitude of 4 mm and frequency of 40 Hz, including an intermediate relaxation of 0.25 s. This injection of energy due to bottom vibration spreads the clumps evenly and allows the ballast particles to fill the possible voids in the system. After the vibration stage, the simulation setup is saved and offers a starting point for the next phase.

3.4.2 Second phase - material update

The restart file of the first phase is then loaded for the second phase of preparation. At first, the material parameters are updated to the set values presented in table 6, followed by relaxation as changing the particle's material of existing interactions can induce a sudden change in contact forces. Afterwards, a plate is inserted directly above the ballast bed. The plate moves downwards with a constant velocity of 0.025 m/s to compress the ballast. As soon as the stress on the plate exceeds 333 kPa (value taken from Kumar et al. [23]), the motion of the plate is reversed. This compacting process is performed for three cycles. After a relaxation for the duration of 0.1 s, all particles above a height of 0.3 m are removed from the ballast bed.

This described compression procedure is repeated to ensure a well-compacted, dense and flat ballast

bed. The resulting ballast bed consists of approximately 9000 clumps (27000 spheres) with a porosity of roughly 0.40. After a relaxation for the duration of 0.25 s, the ballast bed is ready for the next phase.

3.4.3 Third phase - sleeper placement

This phase starts with sleeper implementation on the obtained ballast bed. The sleeper model is initialised in the centre of the box, just above the ballast, and is then dropped under gravity on the ballast bed. The sleeper is allowed to move freely in the lateral and vertical direction, but its longitudinal movement is blocked. Rotational degrees of freedom are not restricted. Following a short relaxation, vertical consolidation forces F_L and F_R are applied. The forces $F_L = F_R$ rise linearly to ensure a smooth consolidation of the sleeper, as demonstrated in blue in figure 26. These vertical forces are applied at the railhead locations situated 0.55 m from each side face of the sleeper. The distance between the railheads is therefore 1.5 m. At each railhead location, the load is distributed to the four nearest nodes on the upper sleeper surface to replicate the force distribution from the rail, as shown in figure 27. When the total force on each railhead reaches 5 kN ($F_{\min}$), it remains constant for another 0.25 s to achieve a balanced state, as shown in orange in figure 26. A restart file is created at the end of this simulation phase to enable simulations for various (cyclic) loading scenarios. The value for $F_{\min}$ was taken from Li et al. [66] and is also considered the lower limit of the cyclic load in the next phase.

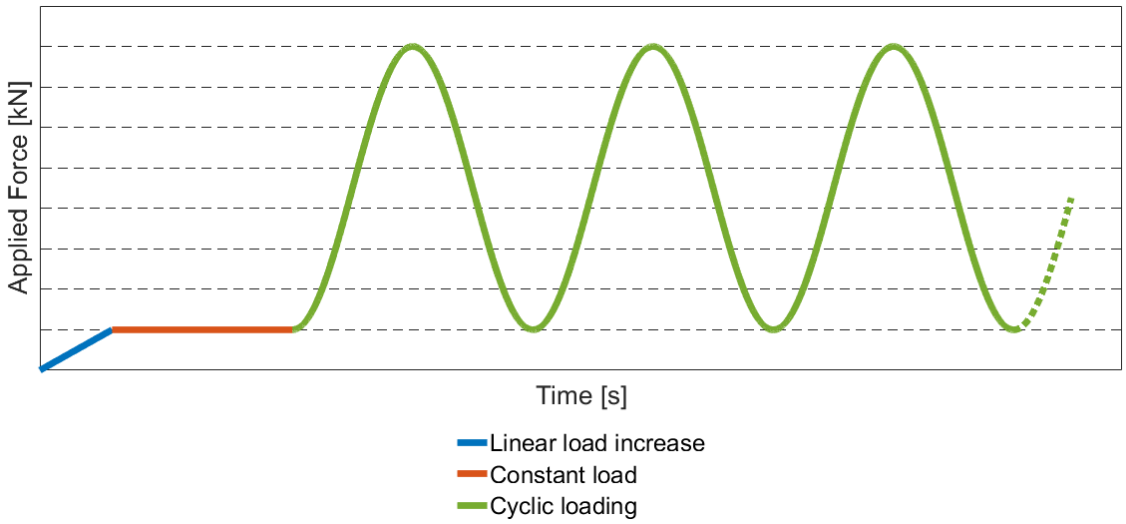

Figure 26: The applied force on the sleeper

3.4.4 Fourth phase - cyclic loading

The state of the consolidated sleeper is then used to perform the main experiment where cyclic loading simulations are performed. The applied force $F_{\text{cyc}}(t)$ is expressed in equation 11 and is visualised in green in figure 26. It depicts a cosine function. The force function replicates the load on each railhead due to a moving vehicle in ideal track conditions. Since a regular straight track is considered in this work, the force on the left railhead F_L is always identical to the force on the right railhead F_R. Different forces on the railheads can be applied, which will enable studying of different loading scenarios in the future. The peak load of $F_{\text{max}} = 40$ kN was applied at each railhead location and was taken from Li et al. [66]. Therefore, the cyclic load alters between 5 kN and 40 kN per railhead, meaning that the force amplitude is $F_a = 17.5$ kN. The low frequency f of 3 Hz is chosen to keep dynamic effects in the system low. The cyclic load is applied on the same nodes as initially done in the third phase, as shown within the simulation setup in figure 27.

$$F_a = 0.5 \cdot (F_{\max} - F_{\min})$$

$$F_{\text{cyc}}(t) = F_{\min} + F_a \cdot [1 - \cos(\, 2\pi f t \,)] \qquad (11) \qquad t \ \ldots \text{ Time [s]}$$

$$F_L(t) = F_R(t) = F_{\text{cyc}}(t)$$

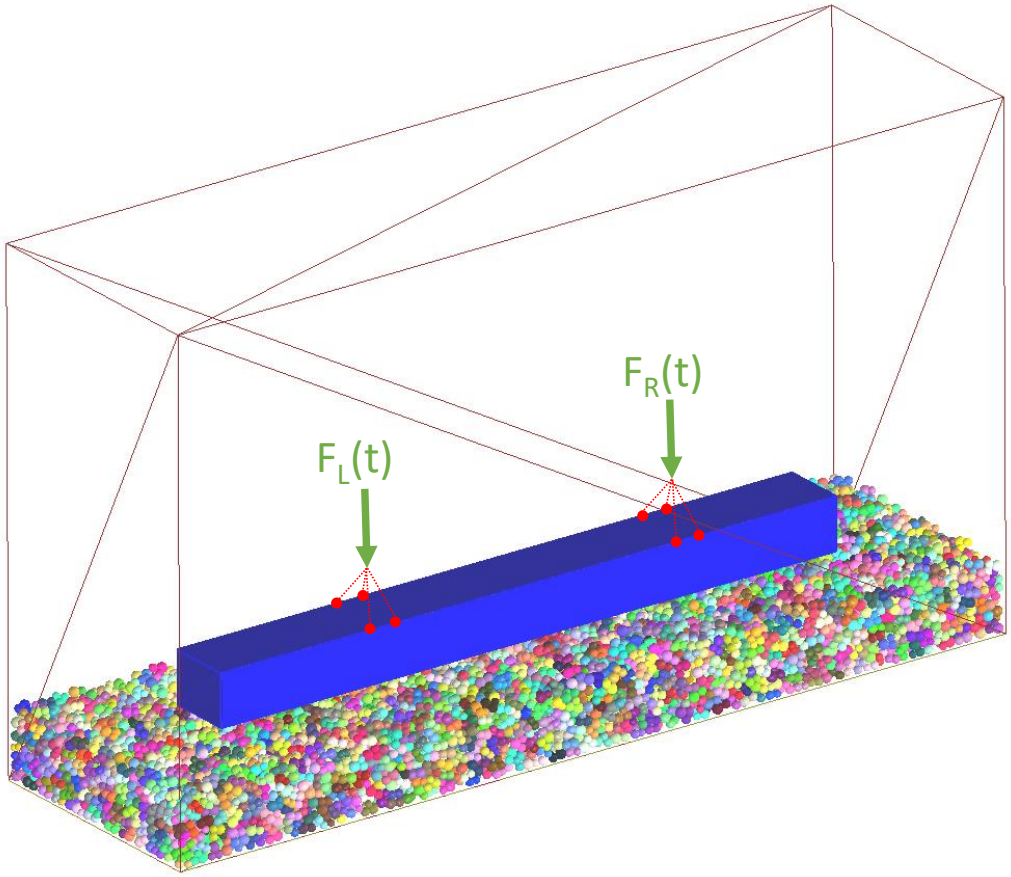

Figure 27: The simulation scenario and force input

4 Results

In this chapter, the results of box-test simulations during cyclic loading over ten cycles are shown and discussed. The loading is applied between 5 kN and 40 kN on each railhead location. At first, the microscopic and macroscopic results are presented, namely the number of contacts between the sleeper and the ballast, sleeper deflection, settlement, and pressure distribution at the sleeper-ballast interface. Afterwards, additional simulations were conducted to analyse the repeatability of the simulation results. Finally, two different loading scenarios were simulated to gain more insight into the effects of force amplitudes on the railway track.

4.1 Main results

4.1.1 Sleeper-ballast contacts

The number of contacts at the sleeper-ballast interface during cyclic loading is shown in figure 28. For the initial (ten) cycles performed in this work, it can be seen that the number of contacts increases with the applied force and does not necessarily return to the initial number after the loading. During the cyclic loading, the number of contacts at the interface varies between approximately 30 and 70 contacts for the lowest and highest load, respectively. Although not an apparent saturation for the number of contacts is seen, it is expected that the number of contacts stabilises after further cyclic loading, as observed in work of Kumar et al. [23], which should be considered in future work.

The number of contacts at the sleeper-ballast interface are of particular importance regarding the settlement. Higher contacts, or higher contact area, lead to lower contact stress, which in turn reduces the sleeper settlement (positive influence) [23]. Therefore, it is crucial to model the sleeper body as an elastic object to carefully analyse the microscopic behaviour at this critical sleeper-ballast interface. Contrary to a rigid sleeper, an elastic DEM sleeper model can help to better understand the contact

and stress situation at the initial and later loading, and thus, can support in developing new track components for reducing the track settlement.

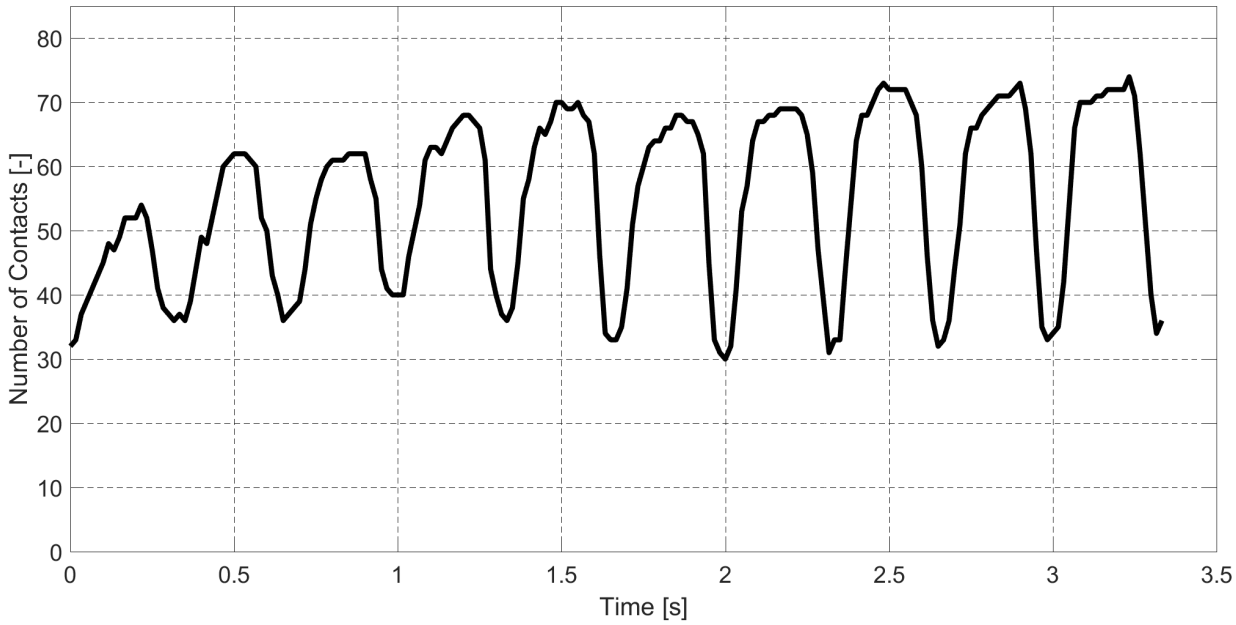

Figure 28: Number of contacts at the sleeper-ballast interface

4.1.2 Sleeper deflection and settlement

The deflection profile of the sleeper at the lowest load (5 kN) of each cycle is shown in figure 29, while the deflection profile at the highest load (40 kN) of each cycle is shown in figure 30. The first cycle is represented in light grey in both plots. The increasing line darkness represents increasing cycles. The locations of the railheads (where the load is applied on the sleeper) are indicated by red dashed lines. It can be seen that in the beginning, already after the consolidation, a W-shaped deflection profile is formed, which is even more pronounced when the peak load is reached.

Along the length of the sleeper, a slight slope (different settlement) can be seen for all loading cycles. This slope is due to the discrete nature of the ballast and differs from idealistic models that consider the ballast as a continuum [47, 50]. Similar asymmetric deflection profiles were observed in long-term

field tests for composite and timber sleepers performed by the U.S. Department of Transportation [51] as presented in section 1.4.2. Due to the discrete particles present in the ballast bed, the porosity (and hence voids) is not uniform as a variation exists in different regions of the ballast bed. Such a situation offers higher settlement in one region compared to another. However, a self-correcting behaviour is expected in later cycles when the less settled part of the sleeper starts to put higher pressure onto the ballast bed, leading to higher settlement in this area. The self-correcting behaviour needs to be confirmed in simulations with a higher amount of cycles in future work. Observations like these are precisely why the combination of an elastic sleeper with a discrete ballast is needed in simulations to deepen the understanding of effects within the track. The inhomogeneous settlement behaviour stays consistent throughout the later cycles. The well-formed W-shape was expected and is therefore in accordance with laboratory experiments from the literature as described in detail in section 1.4.2 [47, 49, 50, 52].

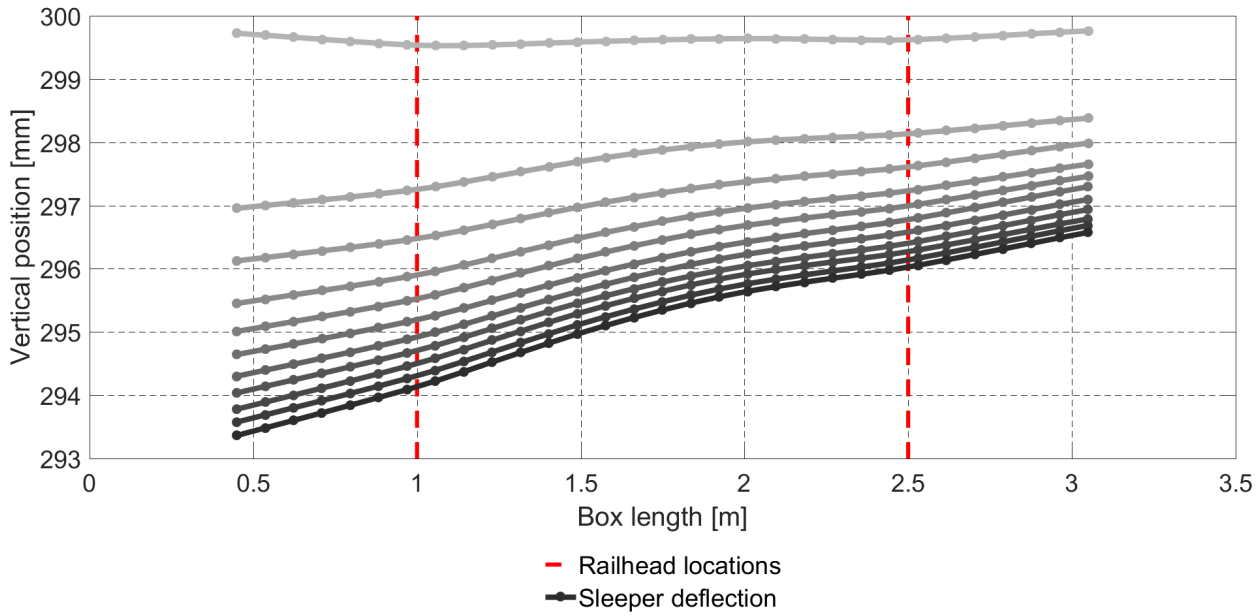

Figure 29: Sleeper deflection at minimal load of 5 kN per railhead for each cycle (increasing darkness represents increasing number of cycles)

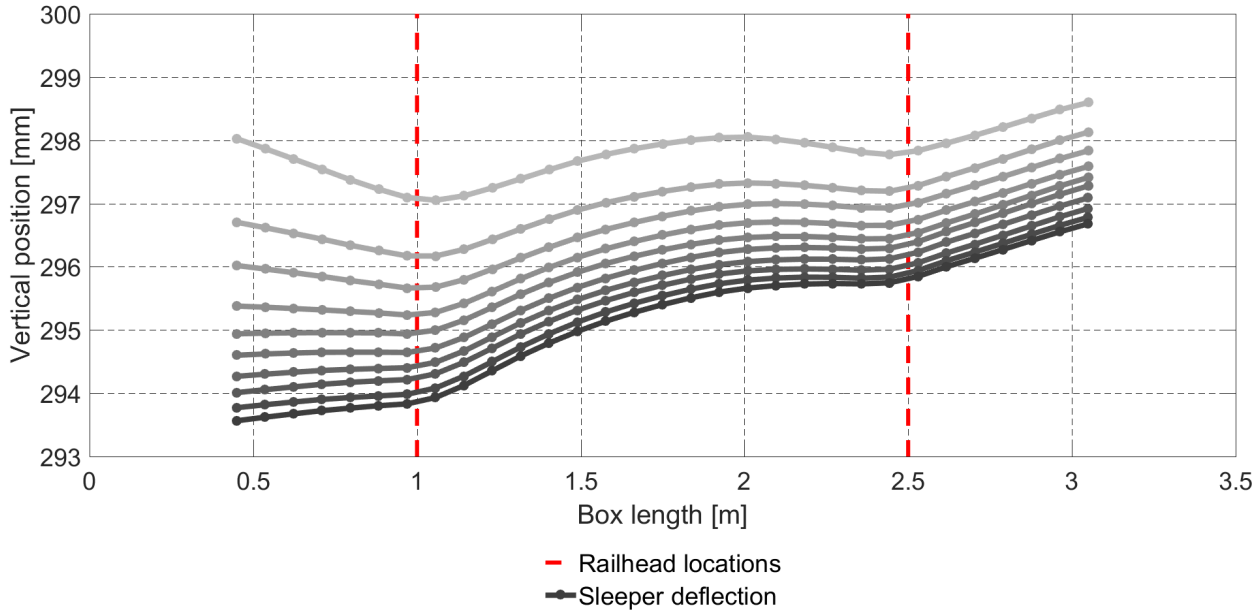

Figure 30: Sleeper deflection at maximum load of 40 kN per railhead for each cycle (increasing darkness represents increasing number of cycles)

In figure 29 and figure 30, it can be seen that the gap between deflection profiles of two consecutive cycles reduces continuously as the simulation progresses, which means that track settlement slows down with cycles. The decreasing settlement rate with load cycles is classical track settlement behaviour as observed in the field and laboratory experiments as well as in several empirical settlement models [37, 38, 97]. The sleeper settlement behaviour below the two railhead locations, obtained by subtracting the present value with the initial sleeper position, is presented in figure 31. This settlement behaviour observed in the simulations resembles the sketch shown in figure 4 in section 1.4 for the initial cycles. The PFM sleeper model in DEM simulations, therefore, helps in qualitatively depicting the settlement behaviour as expected from the literature.

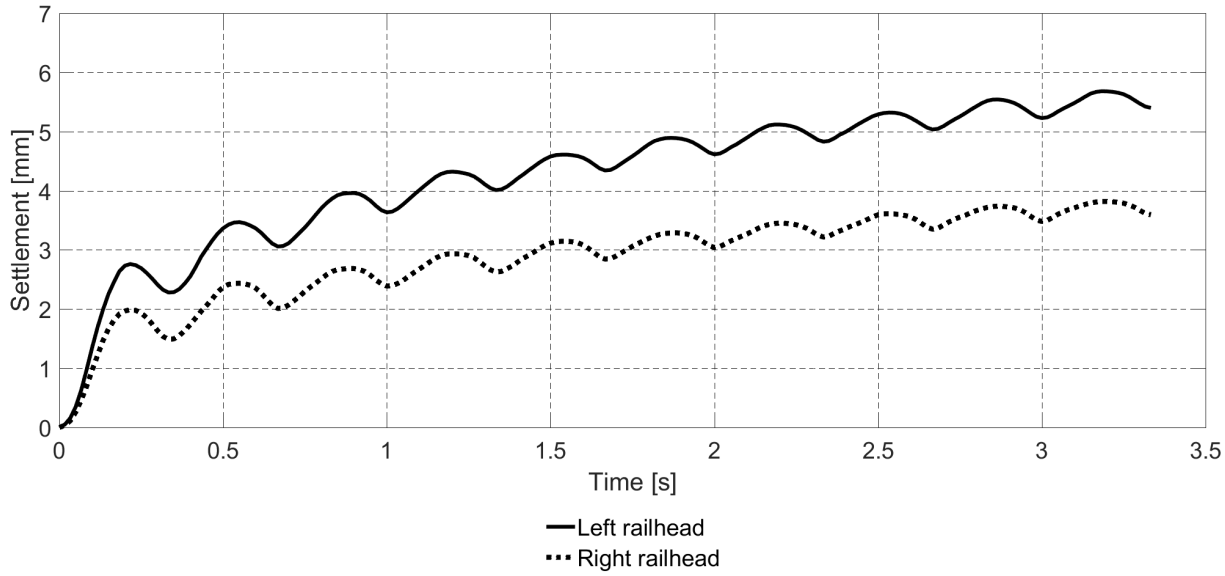

Figure 31: Sleeper settlement behaviour during the load cycles

4.1.3 Pressure distribution

The pressure at the sleeper-ballast interface is an essential quantity that affects the short- and long-term track behaviour. To determine the pressure distribution at the sleeper-ballast interface in simulations, the sleeper is classified into ten equally sized bins along its length. The contact forces of each bin are summed up and divided by the area of the bin to provide the pressure within each bin. The pressure distribution along the sleeper length is shown in figure 32 for the lowest load and figure 33 for the highest load for each cycle.

At the low load, just after the consolidation, the pressure is more or less uniform along the sleeper length, as seen in figure 32. This uniform pressure distribution is mainly because of the low consolation force. For higher loads, a relatively flexible sleeper exerts a less uniform pressure distribution onto the ballast with higher peaks below the rails, as explained in section 1.4.2. Similar behaviour can be observed in figure 33. The higher pressure below the railheads leads to more local ballast settlement near the railhead locations. This behaviour entails a significant sleeper centre binding, meaning

that the ballast beneath the sleeper centre becomes denser and stiffer. This compaction can be seen in figure 32, where the pressure at the centre rises with loading cycles. A self-correcting behaviour is expected with loading cycles since the lesser settlement in the sleeper centre will cause the centre region to transfer more load to the ballast, which will lead to higher pressure and higher settlement at the sleeper centre. This behaviour needs to be verified by simulations with a large number of cycles in future work. The aforementioned observations also indicate that ballast tamping can have significant influence on the sleeper deflection and settlement behaviour. Unlike the uniform ballast compaction in this work, only the ballast directly below the rails is compacted in the tamping process, which can lead to different sleeper deflections (e.g. less centre binding) and, therefore, can affect short- and long-term sleeper settlement behaviour.

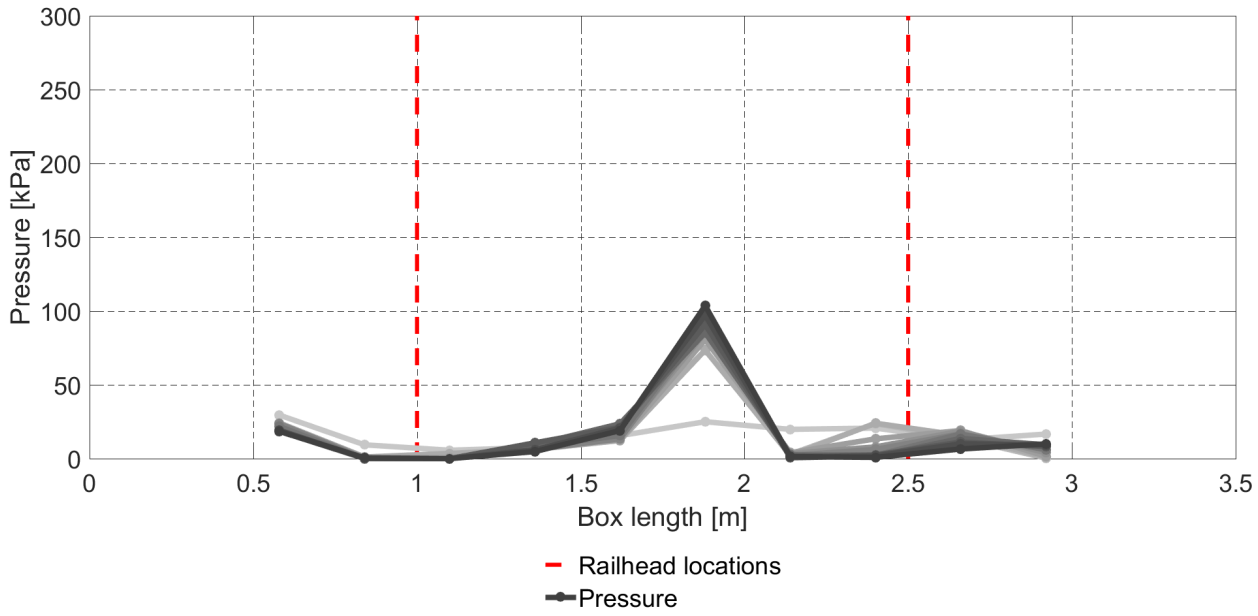

Figure 32: The pressure distribution along the sleeper length at the minimal load of each cycle (increasing darkness represents increasing number of cycles)

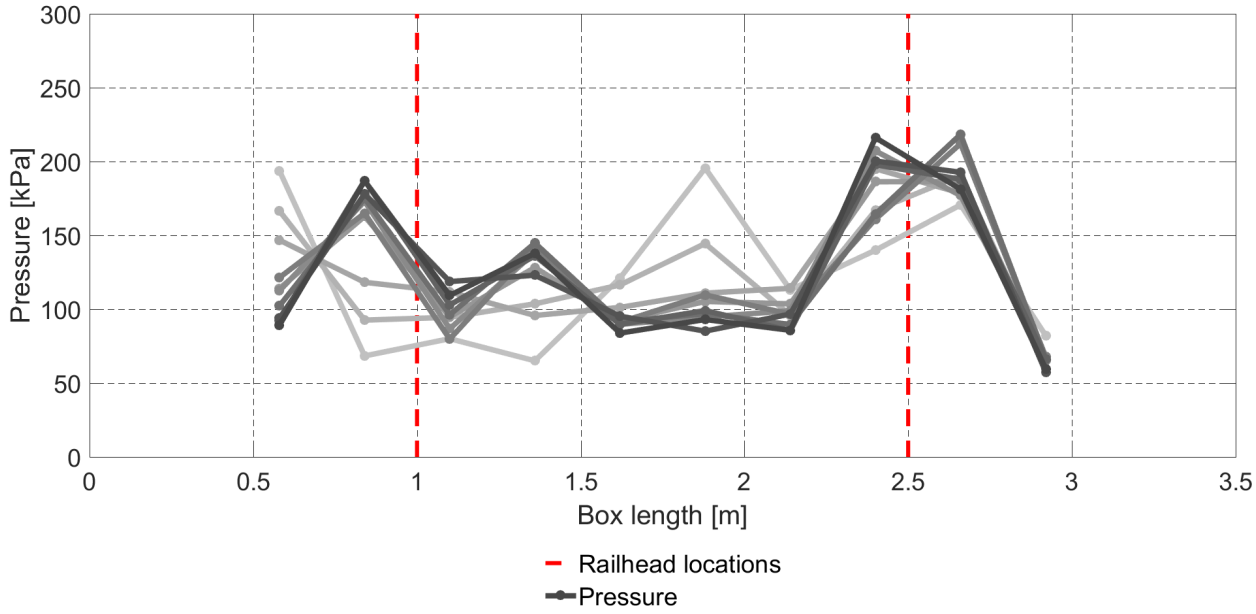

Figure 33: The pressure distribution along the sleeper length at the maximum load of each cycle (increasing darkness represents increasing number of cycles)

It is essential to highlight that the dynamic effects in the system are of minor importance due to the low loading frequency considered in this work, which can be demonstrated by computing the sum of all sleeper-ballast contact forces. At the highest load, the total force applied on the ballast is 80.73 kN due to the external load (40 kN on each railhead) and the sleeper weight (0.73 kN). The net sleeper-ballast contact force is 84.01 kN, which is in the equal order of magnitude as the applied load (4.06 % offset). Thus, the dynamic effects in the simulations have indeed minor influence.

4.2 Additional simulations

In order to check the repeatability of the simulation results, five additional ballast beds were generated and went through the same preparation and cyclic loading steps as described in section 3.4. The only difference in the ballast bed setups is the random generation of the ballast particles in the first phase of the simulation. The bed's mass, height, porosity and the number of particle clumps remained more

or less unchanged for the different ballast beds. The properties of each compacted ballast bed before the sleeper placement are shown in table 7. Bed 1 refers to the initial simulations explained in detail in the previous section.

	Bed mass [kg]	Bed height [mm]	Number of Clumps [-]	Porosity [-]
Bed 1	1476	294.5	8979	0.4043
Bed 2	1479	294.5	8999	0.4013
Bed 3	1479	294.3	8998	0.4015
Bed 4	1482	295.5	9012	0.4014
Bed 5	1478	295.4	8991	0.4033
Bed 6	1478	295.6	8994	0.4019

Table 7: Properties of each ballast bed after the bed preparation, before the sleeper placement

The simulations on the different ballast beds show similar qualitative sleeper-ballast contact behaviour. The evolution of sleeper-ballast contacts with loading cycles for the six ballast beds is shown in figure 34. It can be seen that the observations for the first ballast bed regarding sleeper-ballast contacts are also valid for other ballast beds.

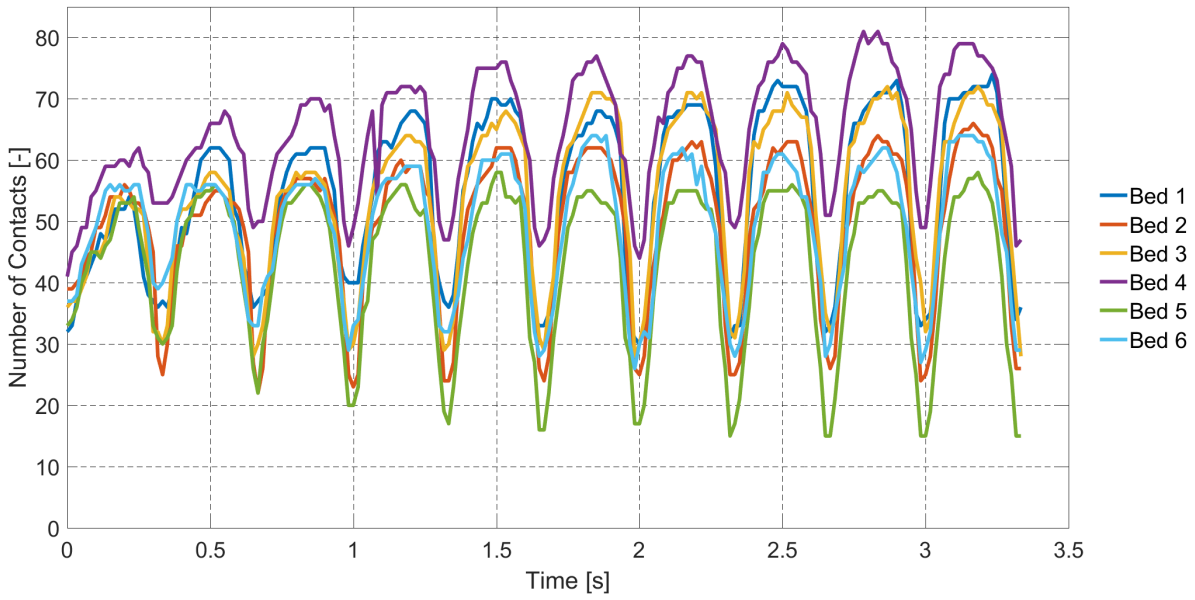

Figure 34: Number of contacts at the sleeper-ballast interface for different beds during repeatability simulations

The number of contacts at this interface strongly depends on the applied force and therefore depicts an oscillating behaviour during cyclic loading. The number of contacts at the highest and lowest load for the individual ballast beds are shown in figure 35 to provide a better overview of the oscillation range. The solid line depicts the upper, while the dotted line depicts the lower values during the loading cycles.

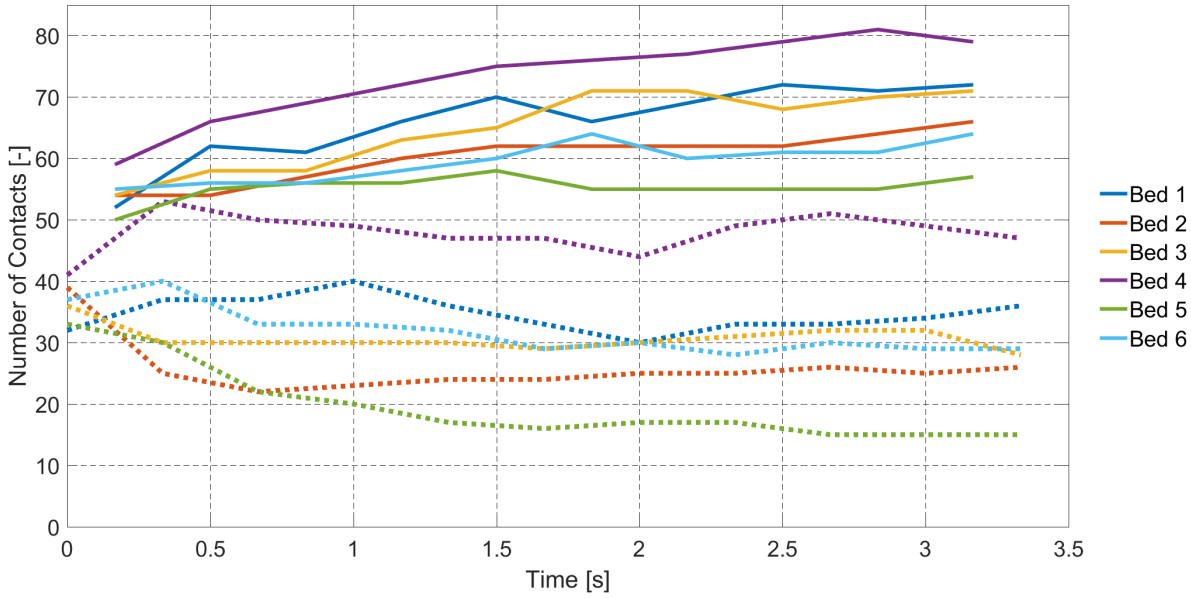

Figure 35: Upper and lower values of the number of contacts at the sleeper-ballast interface for the six different ballast beds. The solid line depicts the contacts at the highest load, while the dotted line depicts the contacts at the lowest load of each cycle.

The sleeper settlement during the load cycles at the two railhead locations for the six ballast beds is presented in figure 36. Solid lines represent left railheads, while dotted lines refer to right railheads. It can be seen that most sleepers have dissimilar settlements at the railhead locations depicting a slope along the sleeper's length. Additionally, it is substantial to note that the settlement values vary a lot for the simulated ballast beds over ten load cycles. This deviation is due to the discrete nature of the ballast stones since the unique arrangement of the particles within each ballast bed can have more or less impact on sleeper settlement.

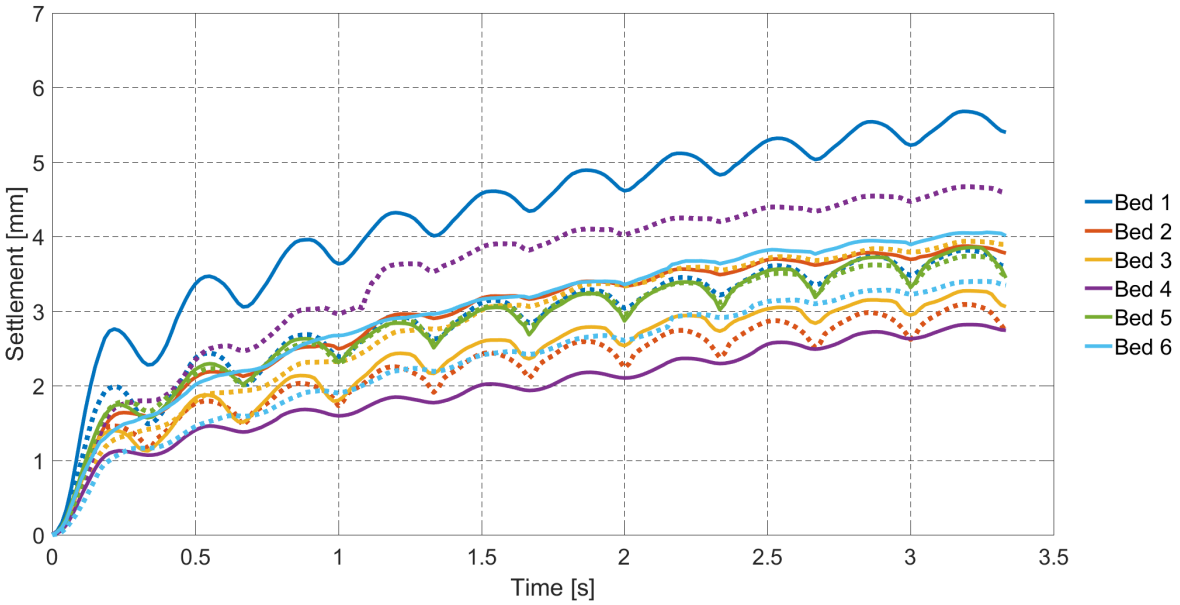

Figure 36: Railhead settlement for the six ballast beds during the repeatability simulations. The solid line depicts the settlement evolution of the left railhead, while the dotted line depicts the settlement evolution of the right railhead.

The results of each ballast bed have shown similar trends for the number of contacts, deflection profile, settlement and pressure distribution. Therefore, sufficient repeatability of the results is given when considering the discrete nature of the ballast bed. A pronounced W-shape deflection profile for all simulated sleepers was observed as well as higher pressure beneath the rails at higher loads and rising pressure below the sleeper centre for lower loads for the considered loading cycles. As all results have shown similar trends that are in agreement with the literature, the proposed modelling method to introduce sleeper elasticity in DEM simulations is considered a viable approach.

4.3 Effects of loading amplitude

Two additional cyclic loading simulations were conducted on bed 1 to investigate the influence of loading amplitude. In one simulation, the maximum load $F_{\max}$ was higher (50 kN), while in the other it was lower (30 kN) than in the initial setup, as presented in equation 11. The lower limit of the

loading (F_{min}) was kept constant at 5 kN for all scenarios. The exact force values are given in table 8. A comparison between the different loading amplitudes regarding the sleeper-ballast contacts is shown in figure 37. The values at the highest loads are represented as solid lines, while the values at the lowest loads are depicted by dotted lines. It can be seen that the number of contacts at the higher loads increases with increasing maximum load F_{max}, which is mainly because of the higher penetration of the sleeper into the ballast bed with higher load leading to a higher number of contacts. As the minimum load F_{min} remained at 5 kN for all simulations, no significant variation in the number of contacts can be observed for the lower loads of the cycles. Clearly, the loading amplitude has a substantial impact on sleeper-ballast contacts.

	F_{min} [kN]	F_{max} [kN]
Increased load	5	50
Initial setup	5	40
Reduced load	5	30

Table 8: The considered loading scenarios on bed 1 using equation 11 for investigating the effects of loading amplitude

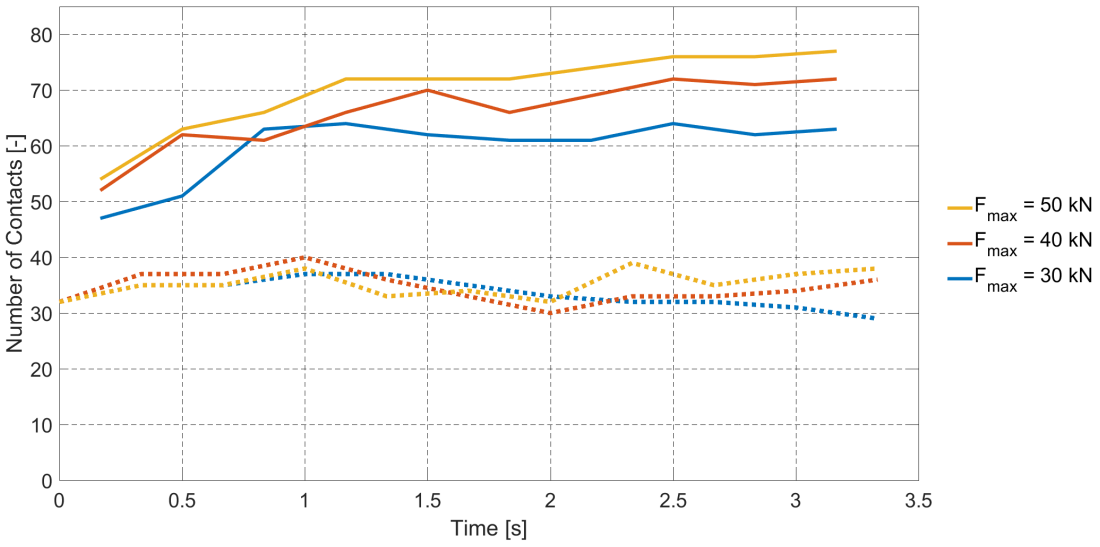

Figure 37: The number of contacts at the sleeper-ballast interface for the three loading scenarios as described in table 8. The solid line depicts the contacts at the highest load, while the dotted line depicts the contacts at the lowest load of each cycle.

The settlement evolution for simulations with different loading amplitudes is shown in figure 38. The sleeper settlement at the left and right railhead location is shown by the solid and dotted lines, respectively. It can be seen that the settlement behaviour increases with loading amplitude. A difference in the settlement behaviour below the two railhead locations is again due to the discrete nature of the ballast bed. The deflection shape of the sleeper at different loading amplitudes remained more or less unchanged during the ten loading cycles applied in this work.

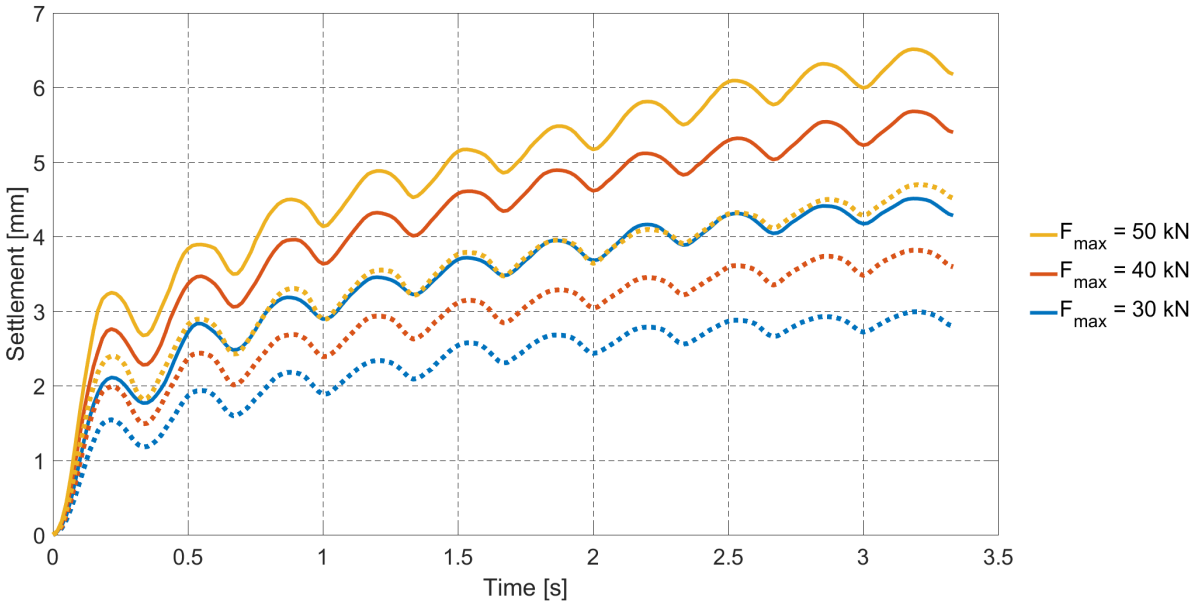

Figure 38: Sleeper settlement at the two railhead locations for the three different loading scenarios described in table 8. The left and right railhead location is shown by the solid and dotted lines respectively.

In figure 39, the pressure at the highest load of the last loading cycle for the three loading scenarios can be seen. The shape of the pressure distribution for all simulated forces remains relatively similar and a higher pressure below the railheads is observed. As expected, the pressure values are higher for a higher applied load and lower for a lower load.

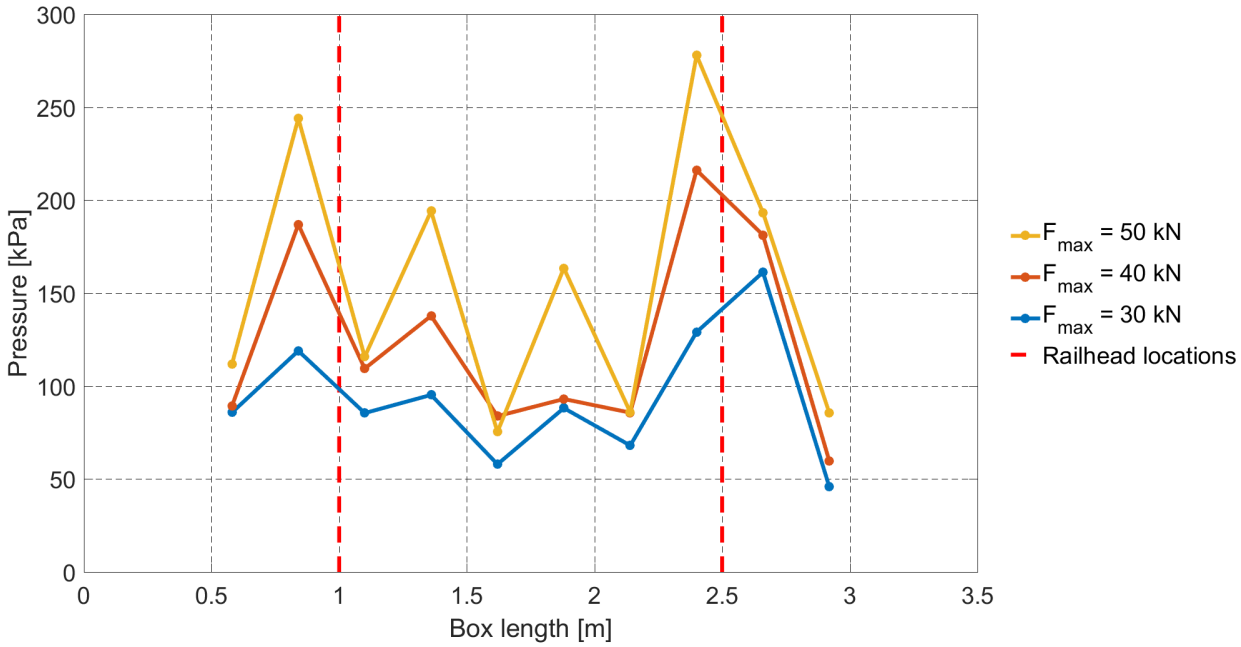

Figure 39: The pressure distribution along the sleeper length at the maximum load of the last cycle for the three loading scenarios as described in table 8.

The observed variation in pressure at the sleeper-ballast interface and sleeper settlement due to the change in loading amplitudes is classical track behaviour. The simulation results are in agreement with the literature and other numerical models and show the impact of elastic sleepers in railway track simulations. Further investigations on the impact of elastic sleepers on settlement can assist in designing sleepers and optimising tracks, thereby reducing the maintenance activities.

5 Concluding remarks

5.1 Summary

This thesis presented a method for incorporating an elastic sleeper body into ballasted railway track discrete element method (DEM) simulations using a relatively novel type of surface modelling technique. The particle facet model (PFM) made it possible to represent an elastic continuum object with a smooth surface as opposed to other models in DEM environments that feature geometrically rough surfaces. The proposed sleeper model is easy to implement and the calibration is straightforward. Additionally, no coupling of two different numerical solvers is needed.

The general structure of ballasted railway tracks is described in the beginning, followed by a comprehensive survey on state-of-art laboratory and numerical research on track settlement and sleeper elasticity. Previously used approaches to integrate elastic sleeper behaviour into DEM simulations are discussed, before the PFM approach is explained in detail. The box-test and its precise assembling of the three components (box, ballast and sleeper) are described, and the simulation procedure is covered. In this study, vertical cyclic loading was applied on the elastic sleeper at two locations representing the positions of the railheads. The same cyclic load was applied on both railheads for ten cycles. The simulations finished within reasonable time and the results regarding the number of contacts at the sleeper-ballast interface, the deflection profile of the sleeper, the sleeper settlement and the pressure distribution along the sleeper length are presented. Finally, the simulation results are discussed, including two additional loading scenarios to study the effects of loading amplitude.

5.2 Conclusions

The proposed modelling method to consider sleeper elasticity in railway track DEM simulations has shown to be a promising approach. The elastic behaviour and the smooth sleeper surface can be

reconstructed accurately for a simple geometrical shape while keeping the required effort low. Moreover, the PFM is available as an open-source subroutine in *Yade* [74] and therefore enables possible modifications for, e.g. regarding the contact modelling.

The results presented in this work are qualitatively similar to the observations from the literature and include insights on physical effects due to the elastic sleeper behaviour. Simulations on additional ballast beds were performed to analyse the effects of initial ballast bed configurations. Besides modelling the sleeper elasticity in the DEM environment, the following conclusions can be drawn for simulations conducted for ten loading cycles:

1. During the cyclic loading, the number of contacts at the sleeper-ballast interface oscillates between a high and low value.
2. The sleeper develops a W-shaped deflection profile when loaded, which becomes even more pronounced under higher loads.
3. The discrete nature of the ballast entails that the loaded sleeper can develop a slope along its length over the ten cycles considered in this work.
4. The sleeper-ballast contact pressure is higher in the region below the railheads than elsewhere at the interface.
5. For the number of cycles investigated, the pressure beneath the sleeper centre increases over the cycles depicting a centre-bound behaviour at the lower loads. This behaviour is expected to be less at later loading cycles since the sleeper centre is the main load bearer and will have higher settlement, thus leading to a self-correcting behaviour.
6. An increase in loading amplitude leads to increased pressure peaks below the railheads, leading to higher settlement.

5.3 Outlook

The thesis presents a viable modelling approach to include elastic sleepers in a DEM environment. Further calibration and adaptations are needed to make the next step from qualitative to quantitative results. The following points need to be considered in order to replicate realistic microscopic and macroscopic track behaviour:

(i) The contact model The contact model should be updated as the used linear contact model does not depict the physical behaviour of ballast for the chosen geometrical representation of sphere clumps. Additionally, the contact behaviour between the sleeper and ballast particles needs to be calibrated and verified.

(ii) The ballast's geometrical representation The increased ballast particle dimension either needs adaptation on the contact model and its parameters, or the initial particle size from Kumar et al. [23] should be considered accepting the fact of increased simulation time.

(iii) The PFacet contact handling The introduction of a virtual sphere to manage the contact between a PFacet and an external particle should be improved to replicate a wall-sphere contact.

Once these points in the DEM setup are successfully modified and validated, further scenarios can be considered in the simulations as this modelling approach offers a broad range of applications. Besides analysing the long-term vertical settlement behaviour by simulating more loading cycles, the lateral resistance and settlement can be investigated where sleeper elasticity is suspected of having a significant impact. This approach can even be enhanced by applying sleeper forces exported from multi-body simulations to depict realistic loading conditions. Even more complex situations, as found in turnouts, are of interest where a longer sleeper can depict a hanging sleeper situation (see also [98–101]), for which an elastic sleeper model is essential.

The applications mentioned above together with recent trends in the railway industry give hope for a bright future for railway researchers to dive even deeper into the ocean of numerical modelling to enable an infrastructure that can withstand the transportation challenges of tomorrow's world.

List of figures

List of tables

References

[1] Wikipedia. *COVID-19 pandemic*. URL: https://en.wikipedia.org/wiki/COVID-19%7B%5C_%7Dpandemic (visited on 2021-09-06).

[2] Tanya Lewis. *How Dangerous Is the Delta Variant, and Will It Cause a COVID Surge in the U.S.? - Scientific American*. 2021. URL: https://www.scientificamerican.com/article/how-dangerous-is-the-delta-variant-and-will-it-cause-a-covid-surge-in-the-u-s/ (visited on 2021-09-01).

[3] Harvard T.H. Chan School of public Health. *Coronavirus and Climate Change*. URL: https://www.hsph.harvard.edu/c-change/subtopics/coronavirus-and-climate-change/ (visited on 2021-09-01).

[4] Wikipedia. *European Green Deal*. URL: https://de.wikipedia.org/wiki/European%7B%5C_%7DGreen%7B%5C_%7DDeal (visited on 2021-09-06).

[5] Sarah Wolf et al. "The European Green Deal — More Than Climate Neutrality". In: *Intereconomics* 56.2 (2021), pp. 99–107. ISSN: 1613964X. DOI: 10.1007/s10272-021-0963-z.

[6] Peter Wormstetter and Matthias Ruete. "Challenges for European Rail". In: *Eur. Energy Policy Pap.* #261.March (2021). URL: https://institutdelors.eu/wp-content/uploads/2021/03/PP261%7B%5C_%7D210329%7B%5C_%7DRail-europeen%7B%5C_%7DRuete%7B%5C_%7DEN.pdf.

[7] *A "European Silk Road": the case for a "big push" in infrastructure investment*. URL: https://european-silk-road.eu/ (visited on 2021-09-06).

[8] ÖBB-Infrastruktur AG. *EYoR - Fragen und Antworten*. URL: https://infrastruktur.oebb.at/de/unternehmen/eyor-europaeisches-jahr-der-schiene/eyor-faq (visited on 2021-09-06).

[9] Wikipedia. *Brennerbasistunnel*. URL: https://de.wikipedia.org/wiki/Brennerbasistunnel (visited on 2021-09-08).

[10] Wikipedia. *Semmering-Basistunnel*. URL: https://de.wikipedia.org/wiki/Semmering-Basistunnel (visited on 2021-09-08).

[11] ÖBB-Infrastruktur AG. *Semmering-Basistunnel*. URL: https://infrastruktur.oebb.at/de/projekte-fuer-oesterreich/bahnstrecken/suedstrecke-wien-villach/semmering-basistunnel (visited on 2021-09-08).

[12] Wikipedia. *Koralmtunnel*. URL: https://de.wikipedia.org/wiki/Koralmtunnel (visited on 2021-09-08).

[13] ÖBB-Infrastruktur AG. *Koralmbahn*. URL: https://infrastruktur.oebb.at/de/projekte-fuer-oesterreich/bahnstrecken/suedstrecke-wien-villach/koralmbahn (visited on 2021-09-08).

[14] WKO. *Schienenverkehr: Struktur, Zukunft und Trends der Branche*. URL: https://www.wko.at/service/aussenwirtschaft/schienenverkehr-branche-struktur-zukunft-trends.html (visited on 2021-09-08).

[15] ÖBB-Infrastruktur AG. *Zukunft Bahn, Zielnetz 2025+*. URL: https://infrastruktur.oebb.at/de/unternehmen/fuer-oesterreich/zukunft-bahn-zielnetz (visited on 2021-09-08).

[16] TU Graz. *Gesamtsystem Bahn: Die Steiermark als internationales Forschungs- und Innovationszentrum*. URL: https://www.tugraz.at/tu-graz/services/news-stories/tu-graz-news/einzelansicht/article/die-zukunft-auf-schienen-gesamtsystem-bahn-die-steiermark-als-internationales-forschungs-und-innovat/ (visited on 2021-09-08).

[17] TU Austria. *Railway System: Styria as International Centre of Research & Innovation*. URL: https://www.tuaustria.ac.at/en/news/news-single-view/gesamtsystem-bahn-die-steiermark-als-internationales-forschungs-und-innovationszentrum (visited on 2021-09-08).

[18] *TU Graz*. URL: https://www.tugraz.at/home/ (visited on 2021-09-08).

[19] *voestalpine AG*. URL: https://www.voestalpine.com/group/de/ (visited on 2021-09-08).

[20] *ÖBB-Infrastruktur AG*. URL: https://infrastruktur.oebb.at/de/ (visited on 2021-09-08).

[21] *Siemens Mobility Austria*. URL: https://www.mobility.siemens.com/at/de.html (visited on 2021-09-08).

[22] *Virtual Vehicle Research GmbH*. URL: https://www.v2c2.at/ (visited on 2021-09-08).

[23] Nishant Kumar et al. "Micro-mechanical investigation of railway ballast behavior under cyclic loading in a box test using DEM: effects of elastic layers and ballast types". In: *Granul. Matter* 21.4 (2019), pp. 1–17. ISSN: 14347636. DOI: 10.1007/s10035-019-0956-9.

[24] Coenraad Esveld. *Modern Railway Track*. Digital Ed. Groenwal: MRT-Productions, 2016. ISBN: 978-1-326-05172-3. URL: www.esveld.com.

[25] Satish Chandra and M.M. Agarwal. *Railway Engineering*. Second Edition. Oxford University Press, 2013. ISBN: 9780198083535. DOI: 10.4018/978-1-7998-7552-9.ch017.

[26] MechTech Guru. *Ballast and Ballast Requirements*. URL: https://www.mechtechguru.com/2021/07/BALLAST%20AND%20BALLAST%20REQUIREMENTS.html (visited on 2021-09-15).

[27] KP-Structures. *Types Of Ballast And Design Of Ballast*. URL: https://www.kpstructures.in/2021/08/types-of-ballast-and-design-of-ballast.html (visited on 2021-09-15).

[28] Wikipedia. *Railroad tie*. URL: https://en.wikipedia.org/wiki/Railroad%7B%5C_%7Dtie (visited on 2021-09-15).

[29] Wikipedia. *Track (rail transport)*. URL: https://en.wikipedia.org/wiki/Track%7B%5C_%7D(rail%7B%5C_%7Dtransport) (visited on 2021-09-15).

[30] Getzner. *Elastic Solutions for use in the Railway Superstructures*. URL: https://www.getzner.com/media/846/download/Brochure%20Elastic%20Solutions%20for%20use%20in%20the%20Railway%20Superstructures%20EN.pdf?v=3 (visited on 2021-09-15).

[31] Agico Group. *Rail pads*. URL: http://www.rail-fastener.com/Rail-Pad.html (visited on 2021-09-15).

[32] P. J. Gräbe et al. "The effects of under-sleeper pads on sleeper-ballast interaction". In: *J. South African Inst. Civ. Eng.* 58.2 (2016), pp. 35–41. ISSN: 10212019. DOI: 10.17159/2309-8775/2016/v58n2a4.

[33] Xing Wang Sheng et al. "Properties of rubber under-ballast mat used as ballastless track isolation layer in high-speed railway". In: *Constr. Build. Mater.* 240 (2020). ISSN: 09500618. DOI: 10.1016/j.conbuildmat.2019.117822.

[34] Sanjay Nimbalkar et al. "Improved Performance of Railway Ballast under Impact Loads Using Shock Mats". In: *J. Geotech. Geoenvironmental Eng.* 138.3 (2012), pp. 281–294. ISSN: 1090-0241. DOI: 10.1061/(asce)gt.1943-5606.0000598.

[35] *Getzner Werkstoffe*. URL: https://www.getzner.com/de (visited on 2021-09-16).

[36] Holger Bach. “Evaluation of attrition tests for railway ballast”. Dissertation. Graz University of Technology, 2013.

[37] Juan Carlos Quezada et al. “Predicting the settlement of coarse granular materials under vertical loading”. In: *Sci. Rep.* 4 (2014), pp. 2–6. ISSN: 20452322. DOI: 10.1038/srep05707.

[38] Taufan Abadi et al. “A Review and Evaluation of Ballast Settlement Models using Results from the Southampton Railway Testing Facility (SRTF)”. In: *Procedia Eng.* 143.Advances in Transportation Geotechnics 3 (2016), pp. 999–1006. ISSN: 18777058. DOI: 10.1016/j.proeng.2016.06.089.

[39] Buddhima Indraratna, Pramod Kumar Thakur, and Jayan S. Vinod. “Experimental and numerical study of railway ballast behavior under cyclic loading”. In: *International Journal of Geomechanics* 10.4 (2010), pp. 136–144. ISSN: 15323641. DOI: 10.1061/(ASCE)GM.1943-5622.0000055.

[40] Anna Christina Neubauer. “The Effect of Petrographic Composition of Railway Ballast on the Los Angeles Abrasion Test”. Master Thesis. Graz University of Technology, 2014.

[41] Buddhima Indraratna et al. “Use of shock mats for mitigating degradation of railroad ballast”. In: *Sri Lankan Geotech. J. -Special Issue Gr. Improv.* 6.1 (2014), pp. 32–41. URL: https://ro.uow.edu.au/eispapers/4943.

[42] Sinniah K. Navaratnarajah, Buddhima Indraratna, and Sanjay Nimbalkar. “Application of Shock Mats in Rail Track Foundation Subjected to Dynamic Loads”. In: *Procedia Eng.* 143.Ictg (2016), pp. 1108–1119. ISSN: 18777058. DOI: 10.1016/j.proeng.2016.06.152.

[43] T. Abadi et al. “Measuring the Area and Number of Ballast Particle Contacts at Sleeper-Ballast and Ballast-Subgrade Interfaces”. In: *Int. J. Railw. Technol.* 4.2 (2015), pp. 45–72. ISSN: 2049-5358. DOI: 10.4203/ijrt.4.2.3.

[44] Mohammad Safari Baghsorkhi et al. “An investigation of railway sleeper sections and under sleeper pads using a box test apparatus”. In: *Proc. Inst. Mech. Eng. Part F J. Rail Rapid Transit* 230.7 (2016), pp. 1722–1734. ISSN: 20413017. DOI: 10.1177/0954409715613818.

[45] Gerald Raymond and Richard Bathurst. “Performance of Large-Scale Model Single Tie-Ballast Systems.” In: *Transp. Res. Rec.* 1131 (1987), pp. 7–14. ISSN: 03611981.

[46] Taufan Abadi et al. “Effect of Sleeper Interventions on Railway Track Performance”. In: *J. Geotech. Geoenvironmental Eng.* 145.4 (2019). ISSN: 1090-0241. DOI: 10.1061/(asce)gt.1943-5606.0002022.

[47] Choman Salih et al. “Effect of bending and compressive modulus of elasticity on the behaviour of timber-alternative railway sleepers supported by ballast”. In: *Case Stud. Constr. Mater.* 15.e00597 (2021). ISSN: 22145095. DOI: 10.1016/j.cscm.2021.e00597.

[48] M Hetényi. *Beams on elastic foundation; theory with applications in the fields of civil and mechanical engineering*. 1946.

[49] Choman Salih et al. “Novel Bending Test Method for Polymer Railway Sleeper Materials”. In: *Polymers (Basel).* 13.1359 (2021). DOI: 10.3390/polym13091359.

[50] E. Ferro, J. Harkness, and L. Le Pen. “The influence of sleeper material characteristics on railway track behaviour: concrete vs composite sleeper”. In: *Transp. Geotech.* 23.100348 (2020). ISSN: 22143912. DOI: 10.1016/j.trgeo.2020.100348.

[51] U.S. Department of Transportation - Federal Railroad Administration. *Performance of plastic composite ties in revenue service*. Tech. rep. May. 2011.

[52] Aran van Belkom. "A simplified method for calculating load distribution and rail deflections in track, incorporating the influence of sleeper stiffness". In: *Adv. Struct. Eng.* 23.11 (2020), pp. 2358–2372. ISSN: 20484011. DOI: 10.1177/1369433220911144.

[53] Yunlong Guo et al. "Calibration for discrete element modelling of railway ballast: A review". In: *Transp. Geotech.* 23.100341 (2020). ISSN: 22143912. DOI: 10.1016/j.trgeo.2020.100341.

[54] Bettina Suhr and Klaus Six. "Parametrisation of a DEM model for railway ballast under different load cases". In: *Granul. Matter* 19.4 (2017), pp. 1–16. ISSN: 14347636. DOI: 10.1007/s10035-017-0740-7.

[55] Bettina Suhr, Stefan Marschnig, and Klaus Six. "Comparison of two different types of railway ballast in compression and direct shear tests: experimental results and DEM model validation". In: *Granul. Matter* 20.4 (2018), pp. 1–13. ISSN: 14347636. DOI: 10.1007/s10035-018-0843-9.

[56] Liang Gao et al. "Discrete element method of improved performance of railway ballast bed using elastic sleeper". In: *J. Cent. South Univ.* 22.8 (2015), pp. 3223–3231. ISSN: 22275223. DOI: 10.1007/s11771-015-2860-8.

[57] Daisuke Nishiura et al. "Computers and Geotechnics Novel discrete element modeling coupled with fi nite element method for investigating ballasted railway track dynamics". In: *Comput. Geotech.* 96.November (2018), pp. 40–54. ISSN: 0266-352X. DOI: 10.1016/j.compgeo.2017.10.011. URL: https://doi.org/10.1016/j.compgeo.2017.10.011.

[58] Yunlong Guo et al. "Effect of sleeper bottom texture on lateral resistance with discrete element modelling". In: *Constr. Build. Mater.* 250 (2020). ISSN: 09500618. DOI: 10.1016/j.conbuildmat.2020.118770.

[59] Weimin Song et al. "Interaction between Railroad Ballast and Sleeper: A DEM-FEM Approach". In: *Int. J. Geomech.* 19.5 (2019). ISSN: 1532-3641. DOI: 10.1061/(asce)gm.1943-5622.0001388.

[60] Xu Zhang, Chunfa Zhao, and Wanming Zhai. "Dynamic Behavior Analysis of High-Speed Railway Ballast under Moving Vehicle Loads Using Discrete Element Method". In: 17.2005 (2017), pp. 1–14. DOI: 10.1061/(ASCE)GM.1943-5622.0000871.

[61] Yunlong Guo et al. "Discrete element modelling of railway ballast performance considering particle shape and rolling resistance". In: *Railw. Eng. Sci.* 28.4 (2020), pp. 382–407. ISSN: 26624745. DOI: 10.1007/s40534-020-00216-9.

[62] Chayut Ngamkhanong et al. "Evaluation of lateral stability of railway tracks due to ballast degradation". In: *Constr. Build. Mater.* 278 (2021), pp. 1–12. ISSN: 09500618. DOI: 10.1016/j.conbuildmat.2021.122342.

[63] Guoqing Jing, Yameng Ji, and Peyman Aela. "Experimental and numerical analysis of anchor-reinforced sleepers lateral resistance on ballasted track". In: *Constr. Build. Mater.* 264 (2020). ISSN: 09500618. DOI: 10.1016/j.conbuildmat.2020.120197.

[64] Morteza Esmaeili, Reza Nouri, and Kaveh Yousefian. "Experimental comparison of the lateral resistance of tracks with steel slag ballast and limestone ballast materials". In: *J. Rail Rapid Transit* 231.2 (2017), pp. 175–184. DOI: 10.1177/0954409715623577.

[65] Linfeng Li et al. "Research on the dynamic behaviour of the railway ballast assembly subject to the low loading condition based on a tridimensional DEM-FDM coupled approach". In: *Constr. Build. Mater.* 218 (2019), pp. 135–149. ISSN: 09500618. DOI: 10.1016/j.conbuildmat.2019.05.102.

[66] Huiqi Li and Glenn McDowell. “Discrete element modelling of two-layered ballast in a box test”. In: *Granul. Matter* 22.4 (2020), pp. 1–14. ISSN: 14347636. DOI: 10.1007/s10035-020-01046-6.

[67] Pouria Mansouri, Jabbar Ali Zakeri, and Saeed Mohammadzadeh. “Numerical and laboratory investigation on lateral resistance of ballasted track with HA110 sleeper”. In: *Constr. Build. Mater.* 301.124133 (2021). ISSN: 09500618. DOI: 10.1016/j.conbuildmat.2021.124133.

[68] Jianxing Liu et al. “Comparative analysis of resistance characteristics of composite sleeper and concrete sleeper in ballast bed”. In: *Constr. Build. Mater.* 300 (2021), p. 124017. ISSN: 09500618. DOI: 10.1016/j.conbuildmat.2021.124017.

[69] G. Q. Jing et al. “Numerical and Experimental Analysis of Lateral Resistance of Biblock Sleeper on Ballasted Tracks”. In: *Int. J. Geomech.* 20.6 (2020), p. 04020051. ISSN: 1532-3641. DOI: 10.1061/(asce)gm.1943-5622.0001689.

[70] Jacob Mortensen et al. “Discrete element modelling of track ballast capturing the true shape of ballast stones”. In: *Powder Technol.* 386 (2021), pp. 144–153. ISSN: 1873328X. DOI: 10.1016/j.powtec.2021.02.066.

[71] M. Sol-Sánchez et al. “Recycling Tire-Derived Aggregate as elastic particles under railway sleepers: Impact on track lateral resistance and durability”. In: *J. Clean. Prod.* 277 (2020). ISSN: 09596526. DOI: 10.1016/j.jclepro.2020.123322.

[72] S. Laryea et al. “Comparison of performance of concrete and steel sleepers using experimental and discrete element methods”. In: *Transp. Geotech.* 1.4 (2014), pp. 225–240. ISSN: 22143912. DOI: 10.1016/j.trgeo.2014.05.001.

[73] J. Stransky and M. Jirasek. “Open Source FEM-DEM Coupling”. In: *18th Int. Conf. Eng. Mech. 2012* (2012), pp. 1237–1251.

[74] Václav Šmilauer et al. “The Yade Project”. In: *Yade Doc. 2nd ed.* (2021). DOI: 10.5281/zenodo.34073. URL: https://yade-dem.org/.

[75] B. Patzák. *OOFEM project home page*. URL: http://www.oofem.org/ (visited on 2021-09-28).

[76] Anna Makouala Effeindzourou et al. “Modelling of deformable structures in the general framework of the discrete element method”. In: *Geotext. Geomembranes* 44.2 (2016), pp. 143–156. ISSN: 02661144. DOI: 10.1016/j.geotexmem.2015.07.015.

[77] Eric Fimbinger. “A Methodology for Dynamic Belt Simulation”. Doctoral Thesis. Montanuniversität Leoben, 2021. DOI: 10.34901/mul.pub.2021.3.

[78] Ardalan Amiri. “Investigation of Discrete Element and Bonded Particle Methods for Modelling Rock Mechanics Subjected to Standard Tests and Drilling”. Master’s Thesis. Politecnico di Milano, 2017.

[79] Bona Park and Ki Bok Min. “Bonded-particle discrete element modeling of mechanical behavior of transversely isotropic rock”. In: *Int. J. Rock Mech. Min. Sci.* 76 (2015), pp. 243–255. ISSN: 13651609. DOI: 10.1016/j.ijrmms.2015.03.014.

[80] Bona Park et al. “Three-dimensional bonded-particle discrete element modeling of mechanical behavior of transversely isotropic rock”. In: *Int. J. Rock Mech. Min. Sci.* 110 (2018), pp. 120–132. ISSN: 13651609. DOI: 10.1016/j.ijrmms.2018.07.018.

[81] D. O. Potyondy and P. A. Cundall. “A bonded-particle model for rock”. In: *Int. J. Rock Mech. Min. Sci.* 41 (2004), pp. 1329–1364. DOI: 10.1016/j.ijrmms.2004.09.011.

[82] Martin Obermayr et al. “A bonded-particle model for cemented sand”. In: *Comput. Geotech.* 49 (2013), pp. 299–313. ISSN: 0266352X. DOI: 10.1016/j.compgeo.2012.09.001.

[83] Prasenjit Ghosh and G. K. Ananthasuresh. “Discrete element modeling of cantilever beams subjected to geometric nonlinearity and particle–structure interaction”. In: *Comput. Part. Mech.* (2020). ISSN: 21964386. DOI: 10.1007/s40571-020-00360-3.

[84] Bruno Chareyre and Pascal Villard. “Dynamic Spar Elements and Discrete Element Methods in Two Dimensions for the Modeling of Soil-Inclusion Problems”. In: *J. Eng. Mech.* 131.7 (2005), pp. 689–698. ISSN: 0733-9399. DOI: 10.1061/(asce)0733-9399(2005)131:7(689).

[85] Franck Bourrier et al. “Discrete modeling of granular soils reinforcement by plant roots”. In: *Ecol. Eng.* 61.1 PARTC (2013), pp. 646–657. ISSN: 09258574. DOI: 10.1016/j.ecoleng.2013.05.002.

[86] C. Xu and D. D. Tannant. “Discrete element modelling of steel wire mesh and rockbolt plate”. In: *Proc. 8th Int. Symp. Gr. Support Min. Undergr. Constr.* April (2016), p. 14.

[87] Marcus Guadagnin Moravia, Pascal Villard, and Delma de Mattos Vidal. “Geogrid pull-out modelling using DEM”. In: *E3S Web Conf.* 92 (2019), pp. 1–6. ISSN: 22671242. DOI: 10.1051/e3sconf/20199213015.

[88] Anna Makouala Effeindzourou et al. “A general method for modelling deformable structures in DEM”. In: *Proc. 4th Int. Conf. Part. Methods - Fundam. Appl. Part. 2015* (2015), pp. 744–754.

[89] Anna Makouala Effeindzourou et al. “Efficient discrete modelling of composite structures for rockfall protection”. In: *Comput. Geotech.* 87.July (2017), pp. 99–114. ISSN: 18737633. DOI: 10.1016/j.compgeo.2017.02.005.

[90] Anna Makouala Effeindzourou. “Numerical Investigation of the Energy Absorption Capacity of Rockfall Protection Measures for Underground Portals”. PhD Thesis. University of Newcastle, 2016.

[91] P. A. Cundall and O. D. L. Strack. “A discrete numerical model for granular assemblies”. In: *Geotechnique* 30.3 (1979), pp. 331–336. ISSN: 17517656. DOI: 10.1680/geot.1980.30.3.331.

[92] D. Weatherley. *ESyS-Particle : An introduction to scripting DEM simulations*. Tech. rep. Earth Systems Science Computational Centre - University of Queensland.

[93] John Harkness et al. “Discrete element simulation of railway ballast: modelling cell pressure effects in triaxial tests”. In: *Granul. Matter* 18.3 (2016), pp. 1–13. ISSN: 14347636. DOI: 10.1007/s10035-016-0660-y.

[94] Christophe Geuzaine and Jean François Remacle. “Gmsh: A 3-D finite element mesh generator with built-in pre- and post-processing facilities”. In: *Int. J. Numer. Methods Eng.* 79.11 (2009), pp. 1309–1331. ISSN: 00295981. DOI: 10.1002/nme.2579.

[95] Meraka Sreerama. “Theoretical Analysis and Experimental Determination of Natural Frequency of Lateral Vibration of a Beam”. In: *Int. J. Adv. Res. Sci. Eng.* 5.01 (2006), pp. 268–276. URL: http://www.ijarse.com/images/fullpdf/1456154642%7B%5C_%7D329S.pdf.

[96] MechaniCalc. *Beam Deflection Tables*. URL: https://mechanicalc.com/reference/beam-deflection-tables (visited on 2021-10-09).

[97] Xu Zhang et al. “Investigation of track settlement and ballast degradation in the high-speed railway using a full-scale laboratory test”. In: *Proceedings of the Institution of Mechanical Engineers, Part F: Journal of Rail and Rapid Transit* 233.8 (2019), pp. 869–881. ISSN: 20413017. DOI: 10.1177/0954409718812231.

[98] A. Lundqvist and T. Dahlberg. “Load impact on railway track due to unsupported sleepers”. In: *Proc. Inst. Mech. Eng. Part F J. Rail Rapid Transit* 219.2 (2005), pp. 67–77. ISSN: 09544097. DOI: 10.1243/095440905X8790.

[99] Mykola Sysyn, Olga Nabochenko, and Vitalii Kovalchuk. “Experimental investigation of the dynamic behavior of railway track with sleeper voids”. In: *Railw. Eng. Sci.* 28.3 (2020), pp. 290–304. ISSN: 26624745. DOI: 10.1007/s40534-020-00217-8.

[100] Guoqing Jing et al. “Micro-analysis of hanging sleeper dynamic interactions with ballast bed”. In: *J. Vibroengineering* 17.1 (2015), pp. 444–455. ISSN: 1392-8716.

[101] Jian Dai, Kok Keng Ang, and Dongqi Jiang. “Moving element analysis of high-speed rail system accounting for hanging sleepers”. In: *MATEC Web Conf.* 148.05007 (2018), pp. 2–7. ISSN: 2261236X. DOI: 10.1051/matecconf/201814805007.